

# Toric Differential Inclusions and a Proof of the Global Attractor Conjecture

Gheorghe Craciun

Department of Mathematics and  
Department of Biomolecular Chemistry  
University of Wisconsin-Madison  
e-mail: `craciun@math.wisc.edu`

version 2

January 12, 2016

## Abstract

The *global attractor conjecture* says that toric dynamical systems (i.e., a class of polynomial dynamical systems on the positive orthant) have a globally attracting point within each positive linear invariant subspace – or, equivalently, complex balanced mass-action systems have a globally attracting point within each positive stoichiometric compatibility class. A proof of this conjecture implies that a large class of nonlinear dynamical systems on the positive orthant have very simple and stable dynamics. The conjecture originates from the 1972 breakthrough work by Fritz Horn and Roy Jackson, and was formulated in its current form by Horn in 1974.

We introduce *toric differential inclusions*, and we show that each positive solution of a toric differential inclusion is contained in an invariant region that prevents it from approaching the origin. We use this result to prove the global attractor conjecture. In particular, it follows that all detailed balanced mass action systems and all deficiency zero weakly reversible networks have the global attractor property.

# 1 Introduction

Any autonomous polynomial dynamical system<sup>1</sup> on the strictly positive orthant  $\mathbb{R}_+^n$  can be represented as

$$\frac{dx}{dt} = \sum_{y \rightarrow y' \in G} k_{y \rightarrow y'} x^y (y' - y) \quad (1)$$

for some geometrically embedded graph<sup>2</sup>  $G$  and some positive constants  $k_{y \rightarrow y'}$ , one for each edge<sup>3</sup>  $y \rightarrow y'$  of  $G$ . (Here  $x^y$  denotes the monomial  $\prod_{i=1}^n x_i^{y_i}$ .) Similarly, any non-autonomous polynomial dynamical system on  $\mathbb{R}_+^n$  can be represented as

$$\frac{dx}{dt} = \sum_{y \rightarrow y' \in G} k_{y \rightarrow y'}(t) x^y (y' - y) \quad (2)$$

for some nonnegative scalar functions  $k_{y \rightarrow y'}(t)$ .

Positive trajectories of (1) and (2) are also trajectories of *mass-action systems* [14]. There is great interest in understanding the *persistence* and *global stability* properties of such dynamical systems [14, 15, 9, 10, 12, 11, 19, 20, 26, 21, 22, 23, 6, 8, 2, 18, 3, 5, 17, 1, 7, 16]. A natural question is the following: for which systems (1) or (2) is it true that trajectories that start in  $\mathbb{R}_+^n$  stay away<sup>4</sup> from the boundary of  $\mathbb{R}_+^n$ ?

Given a polynomial dynamical system, the choice of graph  $G$  above is not unique. We will see that if the graph  $G$  can be chosen such that each edge of  $G$  is contained in a cycle<sup>5</sup>, then any bounded trajectory of (1) must be *persistent* in  $\mathbb{R}_+^n$ . More generally, this is also true for solutions of (2),

<sup>1</sup>or more generally any *power law system* [1], since we do not assume that the coordinates of the vertex points  $y$  are either integer or non-negative. In particular, if vertex points have non-negative integer coordinates we obtain *mass-action systems*.

<sup>2</sup>A *geometrically embedded graph*  $G$  is a finite directed graph whose set of vertices is a finite set  $Y \subset \mathbb{R}^n$ , and each edge of  $G$  is represented by an oriented line segment that connects two vertices  $y, y' \in Y$ . See Fig. 1 for examples.

<sup>3</sup>Inspired by notation from reaction networks, we denote an oriented edge from  $y$  to  $y'$  by  $y \rightarrow y'$ . Moreover, if  $y \rightarrow y'$  is an edge in  $G$  we simply write  $y \rightarrow y' \in G$ .

<sup>4</sup>i.e., for a trajectory  $x(t)$ , we have  $\liminf_{t \rightarrow \infty} x_i(t) > 0$  for all  $i = 1, \dots, n$ . Then we say that the trajectory  $x(t)$  is *persistent*.

<sup>5</sup>or, equivalently, each connected component of  $G$  is strongly connected. If this is the case, we will say that the graph  $G$  is *weakly reversible*.

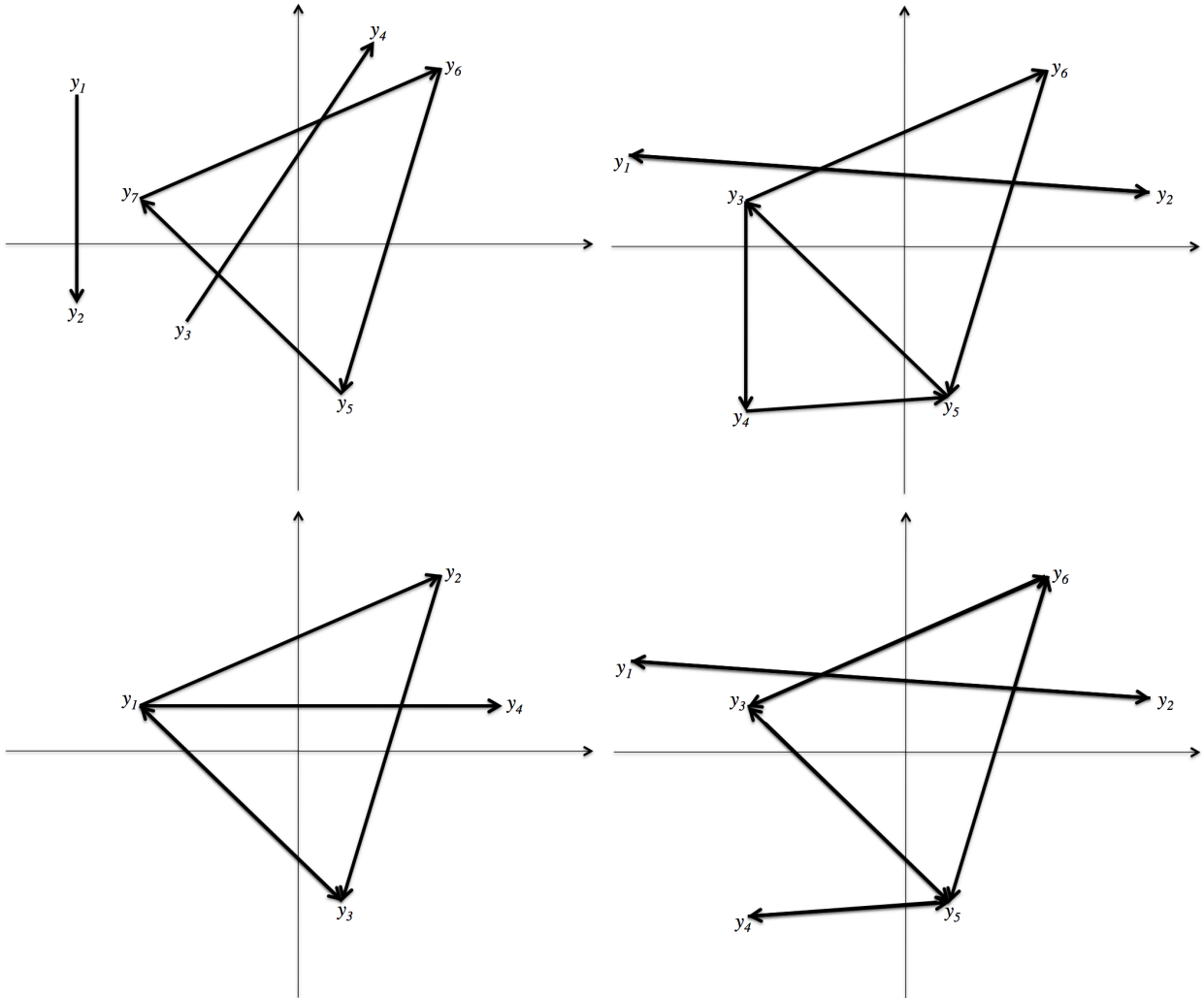


Figure 1: *Four examples of geometrically embedded graphs in  $\mathbb{R}^2$ . Note that, while we do assume that the points  $y_1, \dots, y_k \in \mathbb{R}^2$  are distinct, we do not assume that the line segments (i.e., arrows) representing the vectors  $y_j - y_i$  are disjoint. The two graphs on the right are weakly reversible, and the bottom-right graph is reversible. Although the bottom-left graph is not weakly reversible, it generates dynamical systems (1) which can also be represented by some weakly reversible graph. This is not true for the top-left graph.*

provided that the nonnegative scalar functions  $k_{y \rightarrow y'}(t)$  are *bounded away from zero and infinity*<sup>6</sup>.

In this paper we prove the results mentioned above, and use them to prove the *global attractor conjecture*, which says that toric dynamical systems have a global attractor within any linear invariant subspace<sup>7</sup>. A *toric dynamical system* is a polynomial dynamical system<sup>8</sup> for which there exists a representation of the form (1) that admits a *vertex-balanced equilibrium* in  $\mathbb{R}_+^n$ , i.e., there exists  $x_0 \in \mathbb{R}_+^n$  such that for each vertex  $\bar{y} \in Y$  we have

$$\sum_{y \rightarrow \bar{y} \in G} k_{y \rightarrow \bar{y}} x_0^y = \sum_{\bar{y} \rightarrow y \in G} k_{\bar{y} \rightarrow y} x_0^{\bar{y}}. \quad (3)$$

In other words, if we think of the positive number  $k_{y \rightarrow y'} x^y$  as a flow from the vertex  $y$  to the vertex  $y'$ , then condition (3) says that at each vertex of the graph  $G$ , the sum of all the incoming flows equals the sum of all outgoing flows. The identity (3) implies that the graph  $G$  is weakly reversible [14].

The name “toric dynamical system” has been introduced recently [8] to emphasize the remarkable algebraic properties of these systems, but this class of polynomial dynamical systems has been first studied in depth in the 1972 breakthrough paper of Horn and Jackson [14], where they have been called *complex balanced mass-action systems*. Also in [14] Horn and Jackson have shown that these systems enjoy remarkable stability properties, and in particular *they have a unique positive equilibrium within each linear invariant subspace, and this equilibrium is locally asymptotically stable*. Actually, in [14] Horn and Jackson stated that the unique positive equilibrium within each linear invariant subspace is a *global attractor*<sup>9</sup>, but soon afterwards Horn explained that they have not actually proved this claim, and in 1974 he proposed this global convergence property as a conjecture [15].

The conjecture that toric dynamical systems have a *global attractor* within each linear invariant subspace (or, in the language of Horn, that complex balanced mass-action systems have a global attractor within each reaction simplex) was later called the *Global Attractor Conjecture* [8].

<sup>6</sup> i.e., there exists  $\varepsilon > 0$  such that  $k_{y \rightarrow y'}(t) \in [\varepsilon, \frac{1}{\varepsilon}]$  for all  $t$ .

<sup>7</sup> A *linear invariant subspace* of (1) is an invariant set  $\mathcal{S}_0 = (x_0 + S_0) \cap \mathbb{R}_+^n$ , where  $S_0$  is a linear subset of  $\mathbb{R}^n$ . For toric dynamical systems we will see that  $S_0 = \text{span}\{y' - y : y \rightarrow y' \in G\}$  gives rise to a linear invariant subspace for any  $x_0 \in \mathbb{R}_+^n$ .

<sup>8</sup> or more generally a power law system [1].

<sup>9</sup> i.e., if the positive equilibrium  $x_0$  belongs to the linear invariant subspace  $\mathcal{S}_0$ , then all trajectories that start in  $\mathcal{S}_0$  converge to  $x_0$ .

The global attractor conjecture has resisted efforts for a proof for over four decades, but proofs of many special cases have been obtained during this time, for example [19, 20, 8, 2, 3, 17, 1, 16].

In particular, Craciun, Nazarov and Pantea [1] have recently proved the three-dimensional case, and Pantea has generalized this result for the case where the dimension of the linear invariant subspaces is at most three [16]. Using a different approach, Anderson has proved the conjecture under the additional hypothesis that the graph  $G$  has a single connected component [3], and this result has been generalized by Gopalkrishnan, Miller, and Shiu for the case where the graph  $G$  is strongly endotactic [13].

The results described above do not provide a proof of the global attractor conjecture in full generality, and also do not provide a proof for any of the following three important special cases: (i) the case where  $G$  is *reversible*<sup>10</sup>, (ii) the case where  $G$  is reversible and the system (1) is *detailed balanced*<sup>11</sup>, and (iii) the case where  $G$  is reversible and  $k_{y \rightarrow y'} = 1$  for all  $y \rightarrow y' \in G$ .

The goal of this paper is to introduce *toric differential inclusions*, and to use them to construct a proof of the global attractor conjecture in full generality.

*Toric differential inclusions* are defined as follows. Consider a finite set  $\mathcal{F}$  of polyhedral cones<sup>12</sup> that cover  $\mathbb{R}^n$ , such that  $\mathcal{F}$  is a polyhedral fan<sup>13</sup> [27, 28]. For each cone  $C \in \mathcal{F}$  denote by  $C^o$  the polar cone<sup>14</sup> of  $C$ . Fix some  $\delta > 0$ . For each  $x \in \mathbb{R}^n$  define  $F_{\mathcal{F}, \delta}(x)$  to be the convex cone generated by the union of polar cones  $C^o$  for all  $C \in \mathcal{F}$  such that  $dist(x, C) < \delta$ . Then a

---

<sup>10</sup> i.e., if  $y \rightarrow y' \in G$  then also  $y' \rightarrow y \in G$ .

<sup>11</sup> i.e., we replace the *vertex-balance* equilibrium condition (3) with the more restrictive *edge-balance* equilibrium condition:  $k_{y \rightarrow \bar{y}} x_0^y = k_{\bar{y} \rightarrow y} x_0^{\bar{y}}$  for all  $y \rightarrow \bar{y} \in G$ . This condition says that, at the equilibrium point  $x_0$ , the “forward flux” balances the “reverse flux” for any edge in  $G$ .

<sup>12</sup> A *polyhedral cone* in  $\mathbb{R}^n$  is the intersection of a finite set of half-spaces of  $\mathbb{R}^n$ .

<sup>13</sup> A *polyhedral fan* in  $\mathbb{R}^n$  is a finite set  $\mathcal{F}$  of polyhedral cones such that (i) any face of a cone in  $\mathcal{F}$  is also in  $\mathcal{F}$ , and (ii) the intersection of two cones in  $\mathcal{F}$  is a face of both cones. We say that a polyhedral fan  $\mathcal{F}$  *covers*  $\mathbb{R}^n$  if  $\bigcup_{C \in \mathcal{F}} C = \mathbb{R}^n$ . Simple examples of polyhedral fans  $\mathcal{F}_{\mathcal{H}}$  in  $\mathbb{R}^n$  are given by the polyhedral cones delimited by a finite set  $\mathcal{H}$  of hyperplanes through the origin. This particular case of “hyperplane-generated polyhedral fan” is especially relevant for motivating our definition of toric differential inclusions.

<sup>14</sup> The *polar cone* of a cone  $C \in \mathbb{R}^n$  is the cone  $C^o = \{y \in \mathbb{R}^n \mid x \cdot y \leq 0 \text{ for all } x \in C\}$  [29].

*toric differential inclusion* is a differential inclusion on  $\mathbb{R}_+^n$  given by

$$\frac{dx}{dt} \in F_{\mathcal{F},\delta}(\log x)$$

for some polyhedral fan  $\mathcal{F}$  as above, and some  $\delta > 0$ .

It turns out that, although the global attractor conjecture is formulated in terms of systems of the form (1), we need to understand some properties of systems of the form (2) in order to construct a proof of the conjecture. Therefore, we first prove that we can reduce some systems (2) to toric differential inclusions:

**Theorem A.** *If a polynomial dynamical system has a representation (2) such that  $G$  is weakly reversible and the non-negative functions  $k_{y \rightarrow y'}(t)$  are bounded away from zero and infinity, then it can be embedded<sup>15</sup> in a toric differential inclusion.*

In particular, it follows that if  $G$  is weakly reversible, then (1) can be embedded in a toric differential inclusion for any choice of parameters  $k_{y \rightarrow y'} > 0$ . We then prove that, for any toric differential inclusion  $\mathcal{T}$  and for any positive point  $x_0 \in \mathbb{R}_+^n$ , there exists a hypersurface  $\mathcal{H} \subset \mathbb{R}_+^n$  that separates  $\mathbb{R}_+^n$  into two regions, such that 0 and  $x_0$  are in different regions, and the region that contains the point  $x_0$  is an invariant region for the solutions of  $\mathcal{T}$ :

**Theorem B.** *Toric differential inclusions have an exhaustive set of zero-separating hypersurfaces.*

Then we use this result to conclude that positive trajectories of toric dynamical systems must stay away from the boundary of  $\mathbb{R}_+^n$ :

**Theorem C.** *Toric dynamical systems are persistent.*

Finally, we are able to conclude that the global attractor conjecture is true:

**Theorem D.** *Toric dynamical systems have a globally attracting point within each positive linear invariant subspace.*

## 2 Definitions and notation

As we mentioned in the previous section, some of the main objects of interest in this paper are non-autonomous polynomial dynamical systems of

---

<sup>15</sup> We say that the dynamical system  $\frac{dx}{dt} = f(x)$  is *embedded* into the differential inclusion  $\frac{dx}{dt} \in F(x)$  in the domain  $\Omega$ , if  $f(x) \in F(x)$  for all  $x \in \Omega$ .

the form (2) such that the graph  $G$  is weakly reversible, and the nonnegative scalar functions  $k_{y \rightarrow y'}(t)$  are bounded away from zero and infinity. We will refer to this class of dynamical systems as *k-variable toric dynamical systems*<sup>16</sup>.

More precisely, a *k-variable toric dynamical system* is a dynamical system on  $\mathbb{R}_+^n$  of the form

$$\frac{dx}{dt} = \sum_{y \rightarrow y' \in G} k_{y \rightarrow y'}(t) x^y (y' - y) \quad (4)$$

such that  $G$  is weakly reversible, and there exists a fixed positive number  $\varepsilon$  with  $\varepsilon \leq k_{y \rightarrow y'}(t) \leq \frac{1}{\varepsilon}$  for all  $t$  and for all  $y \rightarrow y' \in G$ .

Note that, under these conditions, solutions of the *k-variable toric dynamical system* above are also solutions of the *differential inclusion* on  $\mathbb{R}_+^n$  given by

$$\frac{dx}{dt} \in F(x), \text{ where } F(x) = \left\{ \sum_{y \rightarrow y' \in G} k_{y \rightarrow y'} x^y (y' - y) \mid \varepsilon \leq k_{y \rightarrow y'} \leq \frac{1}{\varepsilon} \right\}. \quad (5)$$

We will show that solutions of the differential inclusion (5) are also solutions of a type of differential inclusions with rich geometric properties, called *toric differential inclusions*. Later in this section we will define the general notion of toric differential inclusions in  $\mathbb{R}_+^n$ . We first define the class of *polar differential inclusions* in  $\mathbb{R}^n$ .

## 2.1 Polar differential inclusions

If the graph  $G$  is *reversible*, then the equations (4) can be written as

$$\frac{dx}{dt} = \sum_{y \rightleftharpoons y' \in G} \left( k_{y \rightarrow y'}(t) x^y - k_{y' \rightarrow y}(t) x^{y'} \right) (y' - y), \quad (6)$$

by grouping together terms given by an edge  $y \rightarrow y'$  and its reverse  $y' \rightarrow y$ . Then, for each reversible edge  $y \rightleftharpoons y' \in G$ , there is now a single term

---

<sup>16</sup> The name *k-variable toric dynamical system* is due to the fact that any such dynamical system can be obtained from a toric dynamical system by using the same graph  $G$ , and replacing the constants  $k_{y \rightarrow y'}$  with time-dependent non-negative functions  $k_{y \rightarrow y'}(t)$  that are bounded away from zero and infinity.

in the sum (6), which can be thought of as a “tug-of-war” between the forward and reverse terms. Indeed, both the forward and the reverse terms are trying to “push” the state  $x(t)$  of the system along the same line<sup>17</sup>, but in opposite directions. Then, the domain  $\mathbb{R}_+^n$  can be partitioned into three regions: the region where the inequality  $\varepsilon x^y \geq \frac{1}{\varepsilon} x^{y'}$  holds (which implies  $k_{y \rightarrow y'}(t)x^y \geq k_{y' \rightarrow y}(t)x^{y'}$ ), the region where the inequality  $\frac{1}{\varepsilon} x^y \leq \varepsilon x^{y'}$  holds (which implies  $k_{y \rightarrow y'}(t)x^y \leq k_{y' \rightarrow y}(t)x^{y'}$ ), and an *uncertainty region* where neither one of these two inequalities are satisfied, and either one of the two terms  $k_{y \rightarrow y'}(t)x^y$  and  $k_{y' \rightarrow y}(t)x^{y'}$  may win the tug-of-war, due to the fact that  $k_{y \rightarrow y'}(t)$  and  $k_{y' \rightarrow y}(t)$  may take any values between  $\varepsilon$  and  $\frac{1}{\varepsilon}$ . Some concrete examples can be found in Section 3 of [1]. In particular, note that if one term does win the tug-of-war, then the direction of the sum of the two terms is *towards* the uncertainty region, and also towards the hypersurface  $x^y = x^{y'}$  in  $\mathbb{R}_+^n$ .

The simplest way to understand how these regions adjoin each other is to look at them in  $\mathbb{R}^n$  instead of  $\mathbb{R}_+^n$ , after applying a logarithmic transformation. If we denote  $X = \log x$ , then the hypersurface  $x^y = x^{y'}$  becomes the hyperplane  $(y' - y) \cdot X = 0$ . Moreover, the uncertainty region described above becomes just the set of points at distance  $< \delta = \frac{2|\log \varepsilon|}{\|y' - y\|}$  from this hyperplane. Note also that the direction given by the vector  $y' - y$  is exactly the direction orthogonal to the hyperplane  $(y' - y) \cdot X = 0$ .

Therefore, if the graph  $G$  consists of a *single* reversible edge  $y \rightleftharpoons y'$ , then the dynamics of the system (6) at a point  $x$  can be described as follows: we know that  $x$  will move along a line of support vector  $(y' - y)$ , and we are able to specify one direction or another by mapping  $x$  to  $X = \log x$ , and checking whether the distance between  $X$  and the hyperplane  $(y' - y) \cdot X = 0$  is  $\geq \delta$ . Moreover, if we *can* specify this direction, then it is always the direction *towards* (and not away from) this hyperplane, and orthogonal to it.

This characterization has the advantage that it can be carried over to the more general case, where  $G$  contains *several* reversible edges. In that case we have several tug-of-wars going on at the same time, but for each one of them we can specify the winning direction (if any) at  $x$  by calculating the distance between  $X = \log x$  and some hyperplane in  $\mathbb{R}^n$ . Depending on whether  $X$  falls outside an uncertainty region or not, each reversible edge  $y \rightleftharpoons y'$  of  $G$  contributes one or two resultant vectors (if one, then it is either  $y' - y$  or  $y - y'$ , and if two, then they are  $\pm(y' - y)$ ).

---

<sup>17</sup> i.e., a line whose direction is given by the vector  $y' - y$ .



It follows that any system (6) can be embedded into a differential inclusion on  $\mathbb{R}_+^n$  given by a set  $\mathcal{H}$  of hyperplanes in  $\mathbb{R}^n$  and a number  $\delta > 0$ , as follows. For each  $x \in \mathbb{R}_+^n$  we define  $F_{\mathcal{H},\delta}(\log x)$  to be the convex cone generated by vectors orthogonal to the hyperplanes of  $\mathcal{H}$ , in the direction that goes from the point  $X = \log x$  towards each hyperplane, and also the opposite direction if  $X$  is at distance  $< \delta$  from some hyperplane. If  $X$  does not belong to any uncertainty region, then  $F_{\mathcal{H},\delta}(\log x)$  is defined to be exactly the *polar cone*  $C^o$  of a cone  $C$  bounded by a subset of hyperplanes<sup>18</sup> from  $\mathcal{H}$ . Moreover, if  $X$  does belong to some uncertainty regions, then we can still describe  $F_{\mathcal{H},\delta}(\log x)$  in terms of polar cones, by including not just the polar of the largest cone of  $\mathcal{F}(\mathcal{H})$  that contains  $X$ , but also the polar of each cone of  $\mathcal{F}(\mathcal{H})$  that is at distance  $\leq \delta$  from  $X$ .

Of course, not all polyhedral fans are determined by a set of hyperplanes as above. Nevertheless, we can generalize the construction described above to define *polar differential inclusions* given by a polyhedral fan  $\mathcal{F}$  in  $\mathbb{R}^n$ , as described in the previous section: we define  $F_{\mathcal{F},\delta}(X)$  to be the convex cone generated by the union of polar cones  $C^o$  for all  $C \in \mathcal{F}$  such that  $\text{dist}(X, C) < \delta$ .

## 2.2 Toric differential inclusions

Polar differential inclusions can produce sets of cones that contain the right-hand-side of the vector fields (4) for reversible  $G$ , but they are defined on  $\mathbb{R}^n$ , while the system (4) is defined on  $\mathbb{R}_+^n$ . To obtain a proper generalization we need to introduce *toric differential inclusions*, which are obtained from polar differential inclusions by a logarithmic change of variable: a toric differential inclusion given by a polyhedral fan  $\mathcal{F}$  in  $\mathbb{R}^n$  is a differential inclusion on  $\mathbb{R}_+^n$  given by

$$\frac{dx}{dt} \in F_{\mathcal{F},\delta}(\log x) \tag{7}$$

where  $F_{\mathcal{F},\delta}$  is a polar differential inclusion as defined above.

Due to the way this definition is related to the system (6), it follows that  $k$ -variable toric dynamical systems (4) can be embedded into polar differential inclusions, provided that the graph  $G$  is reversible.

---

<sup>18</sup> the cone  $C$  is the largest cone that contains the point  $X$  within the polyhedral fan  $\mathcal{F}(\mathcal{H})$  determined by the set of hyperplanes  $\mathcal{H}$ . The convex cone generated by the “outer normal” vectors orthogonal to the hyperplane faces of  $C$  is its polar cone  $C^o$  [28].

As we discussed above, for a reversible graph  $G$ , the polyhedral fan  $\mathcal{F}$  could be chosen simply as the fan generated by the set of hyperplanes that are orthogonal to the vectors  $y' - y$  for  $y \rightarrow y' \in G$ .

We need to remove this strong reversibility assumption, in order to be able to address the global attractor conjecture in full generality. In the next section we explain how to find such a polyhedral fan for any *weakly* reversible graph  $G$ .

### 3 Connection between $k$ -variable toric dynamical systems and toric differential inclusions

As we discussed in the previous section, the simplest examples of polar differential inclusions are generated by polyhedral fans  $\mathcal{F}_{\mathcal{H}}$  that are determined by a finite set  $\mathcal{H}$  of hyperplanes<sup>19</sup> that pass through the origin. Then, the simplest examples of toric differential inclusions are also generated by polyhedral fans  $\mathcal{F}_{\mathcal{H}}$  as above. We will refer to this class of toric differential inclusions as *hyperplane-generated toric differential inclusions*.

We have seen in the previous section that any *reversible*  $k$ -variable toric dynamical system in  $\mathbb{R}_+^n$  can be embedded into a (hyperplane-generated) toric differential inclusion. Here we show that a similar fact is true for all  $k$ -variable toric dynamical systems<sup>20</sup>.

**Theorem 3.1.** *Consider a  $k$ -variable toric dynamical system (4). Then this system can be embedded into a toric differential inclusion.*

*Proof.* Assume first that the weakly reversible graph  $G$  is made up of a single oriented cycle. If our single-cycle graph is given by  $y_1 \rightarrow y_2 \rightarrow \dots \rightarrow y_r \rightarrow y_1$ , then the  $k$ -variable toric dynamical system it generates is of the form

$$\frac{dx}{dt} = \sum_{i=1}^r k_i(t) x^{y_i} (y_{i+1} - y_i), \quad (8)$$

where  $y_{r+1} = y_1$  and  $\varepsilon_0 \leq k_i(t) \leq \frac{1}{\varepsilon_0}$  for some  $\varepsilon_0 > 0$ .

---

<sup>19</sup> i.e.,  $\mathcal{F}_{\mathcal{H}}$  consists of all the cones delimited by hyperplanes in  $\mathcal{H}$ .

<sup>20</sup> In order to prove the global attractor conjecture we need to construct zero-separating surfaces for all  $k$ -variable toric dynamical systems (not just for the reversible ones). Theorem 3.1 implies that it is sufficient to construct zero-separating surfaces for toric differential inclusions.

Consider the set  $\mathcal{L}$  of lines through the origin in the direction of vectors  $y_i - y_j$  for all  $i \neq j$ , and denote by  $\mathcal{H}$  the set of all hyperplanes that are orthogonal complements of lines in  $\mathcal{L}$ <sup>21</sup>. Denote by  $\mathcal{F}_{\mathcal{H}}$  the polyhedral fan generated by the set of hyperplanes  $\mathcal{H}$ , and, for  $\delta > 0$ , denote by  $\mathcal{T}_{\mathcal{H},\delta}$  the corresponding hyperplane-generated toric differential inclusion. We will show that there exists  $\delta_0 > 0$  such that the single-cycle  $k$ -variable toric dynamical system (8) is embedded in the toric differential inclusion  $\mathcal{T}_{\mathcal{H},\delta_0}$ .

Choose  $\delta_0 > 0$  large enough such that the uncertainty regions given by the *reversible* edges  $y_i \rightleftharpoons y_j$  and  $\varepsilon_0$  are contained within the uncertainty regions of the toric differential inclusion  $\mathcal{T}_{\mathcal{H},\delta_0}$ .

Fix a point  $x \in \mathbb{R}_+^n$  such that  $X = \log x$  belongs to some cone  $C$  in  $\mathcal{F}_{\mathcal{H}}$ , and does *not* belong to any uncertainty region of  $\mathcal{T}_{\mathcal{H},\delta_0}$ . In particular, it follows that the cone  $C$  has dimension  $n$ , otherwise  $X$  would be contained in some hyperplane in  $\mathcal{H}$ , which in turn would be contained in an uncertainty region of  $\mathcal{T}_{\mathcal{H},\delta_0}$ . We want to show that the right-hand-side of (8) is contained in the dual cone  $C^\circ$ .

Consider a vector  $w$  in the interior of  $C$ , and project  $y_1, y_2, \dots, y_r$  on the line  $l_w$  that passes through the origin in the direction given by  $w$ . Then no two projections are the same, because  $w$  does not belong to any of the hyperplanes in  $\mathcal{H}$ . We now give a second set of names to the vectors  $y_1, y_2, \dots, y_r$ , say  $v_1, v_2, \dots, v_r$ , to record the *distance to the origin* of the projections along the line (i.e., if the projection of  $y_{i_1}$  is the closest to origin, then  $v_1 = y_{i_1}$ , and if the projection of  $y_{i_2}$  is the second closest to origin, then  $v_2 = y_{i_2}$ , and so on). Note that, since the interior of  $C$  is disjoint from all the hyperplanes in  $\mathcal{H}$ , it follows that the new names  $v_1, v_2, \dots, v_r$  do *not* depend on the particular choice of vector  $w$  in the interior of  $C$ . In other words, the dot products  $(v_{l+1} - v_l) \cdot w$  are all *negative* numbers, for all  $w$  in the interior of  $C$ . Therefore, the vectors  $v_2 - v_1, v_3 - v_2, \dots, v_r - v_{r-1}$  belong to  $C^\circ$ .

So, in order to show that the right-hand side of (8) is included in  $C^\circ$ , it is enough to show that it can be written as a positive linear combination of the vectors  $v_2 - v_1, v_3 - v_2, \dots, v_r - v_{r-1}$ .

Note that  $(i_1, i_2, \dots, i_r)$  is a permutation of  $(1, 2, \dots, r)$ . If we denote the inverse permutation by  $(j_1, j_2, \dots, j_r)$ , it follows that  $y_1 = v_{j_1}$ ,  $y_2 = v_{j_2}$ , and so on.

---

<sup>21</sup>i.e., a hyperplane belongs to  $\mathcal{H}$  iff it is orthogonal to a line in  $\mathcal{L}$ .

Then we have  $y_2 - y_1 = v_{j_2} - v_{j_1}$ . If  $j_2 > j_1$  we write

$$y_2 - y_1 = \sum_{l=j_1}^{j_2-1} (v_{l+1} - v_l),$$

and if  $j_2 < j_1$  we write

$$y_2 - y_1 = - \sum_{l=j_2}^{j_1-1} (v_{l+1} - v_l),$$

We do the same for  $y_3 - y_2$ ,  $y_4 - y_3$ , and so on. This way, we write each difference  $y_{i+1} - y_i$  from the right-hand-side of (8) in terms of the vectors  $\pm(y_{l+1} - y_l)$ , with  $l = 1, 2, \dots, r-1$ . Therefore we can re-group terms to obtain

$$\frac{dx}{dt} = \sum_{i=1}^{r-1} \Phi_i (v_{i+1} - v_i), \quad (9)$$

where  $\Phi_i$  is a sum of several terms of the form  $k_i x^{v_i}$ , with various signs.

Note now that the positive terms inside  $\Phi_l$  correspond to edges of the form  $v_m \rightarrow v_n$  with  $m \leq l < n$ , and negative terms inside  $\Phi_l$  correspond to edges of the form  $v_m \rightarrow v_n$  with  $n \leq l < m$ . This means that the positive terms inside  $\Phi_l$  contain  $k_i x^{v_i}$  with  $i \leq l$ , and the negative terms inside  $\Phi_l$  contain  $k_i x^{v_i}$  with  $i > l$ . Since  $\log x \in C$  (and is not in an uncertainty region), and due to our choice of  $\delta_0$ , it follows that  $k_1 x^{v_1} < k_2 x^{v_2} < \dots < k_r x^{v_r}$ . Therefore, the sum of the positive terms inside  $\Phi_l$  dominates the sum of the negative terms inside  $\Phi_l$ , for each  $l^{22}$ . In conclusion, the right-hand-side of (9) (and therefore (8)) is a positive linear combination of the vectors  $v_{l+1} - v_l$ , for  $1 \leq l \leq r-1$ , so it belongs to  $C^o$ .

If  $x$  *does* belong to an uncertainty region of the toric differential inclusion  $\mathcal{T}_{\mathcal{H}, \delta_0}$ , then denote by  $F(x)$  the cone of  $\mathcal{T}_{\mathcal{H}, \delta_0}$  at  $x$ . It follows that the maximal linear subspace contained in  $F(x)$  has dimension  $\geq 1$  in  $\mathbb{R}^n$ . We project the problem on the orthogonal complement of that subspace, and then we reason the same way as above<sup>23</sup>. This gives us the desired conclusion for the case when  $G$  is made up of a single oriented cycle.

---

<sup>22</sup> note that the number of positive terms inside  $\Phi_l$  is the same as the number of negative terms inside  $\Phi_l$ , because the graph  $G$  is a cycle.

<sup>23</sup> When projecting on the smaller dimensional subspace, the graph  $G$  is replaced by its projection  $\tilde{G}$ . All vertices of  $G$  that project to the same vertex of  $\tilde{G}$  are interchangeable

If the weakly reversible graph  $G$  is *not* a single oriented cycle, then we write it as a union of cyclic graphs,  $G = \bigcup_{i=1}^g G_i$ , and we can argue as above for each such  $G_i$ . We obtain that the  $k$ -variable toric dynamical systems given by the cycle  $G_i$  are embedded in toric differential inclusions generated by some set of hyperplanes  $\mathcal{H}_i$ . Note now that the right-hand-side of a  $k$ -variable toric dynamical system given by  $G$  can be decomposed into a sum of terms, such that each term is of the form<sup>24</sup> given by the right-hand-side of a  $k$ -variable toric dynamical system determined by  $G_i$ . Then we conclude that any  $k$ -variable mass-action system given by  $G$  can be embedded into a toric differential inclusion generated by the set of hyperplanes  $\mathcal{H} = \bigcup_{i=1}^g \mathcal{H}_i$ .  $\square$

## 4 Construction of zero-separating surfaces for toric differential inclusions

In this section we show that for any toric differential inclusion  $\mathcal{T}$  on  $\mathbb{R}_+^n$  and any small enough neighborhood  $V_0$  of the origin in  $\mathbb{R}^n$  there exists a *zero-separating surface*, i.e., a hypersurface  $Z_{\mathcal{T}, V_0}$  such that  $\mathbb{R}_+^n \setminus Z_{\mathcal{T}, V_0}$  is the union of two disjoint and connected open sets  $Z_{\mathcal{T}, V_0}^0$  and  $Z_{\mathcal{T}, V_0}^1$ , such that  $Z_{\mathcal{T}, V_0}^0 \subset V_0$ ,  $Z_{\mathcal{T}}^1$  is an invariant region of  $\mathcal{T}$ , and the closure of  $Z_{\mathcal{T}}^1$  does not contain the origin.

Then, it will follow that any solution of  $\mathcal{T}$  with initial condition  $x_0 \in \mathbb{R}_+^n$  must be contained in some invariant region  $Z_{\mathcal{T}}^1$  as described above, and in particular it cannot have an  $\omega$ -limit point at the origin.

**Remark 4.1.** *Note that, if we want to construct zero-separating surfaces for toric differential inclusions in  $\mathbb{R}_+^n$ , it is actually sufficient to focus on hyperplane-generated toric differential inclusions, because for any toric differential inclusion  $\mathcal{T}_1$  there exists a hyperplane-generated toric differential inclusion  $\mathcal{T}_2$ , such that  $\mathcal{T}_1$  is embedded in  $\mathcal{T}_2$  (for example, we can choose  $\mathcal{T}_2$  to be generated by the set of hyperplanes  $\mathcal{H}$  that consists of all the support*

---

with each other when checking that the right-hand-side of (8) is contained in the (degenerate) cone  $F(x)$ , because the projections are done along linear subspaces contained in  $F(x)$ .

<sup>24</sup> We may have to use smaller  $\varepsilon_i$  values for the terms in the decomposition, because the same edge of  $G$  may belong to several graphs  $G_i$ .

hyperplanes of the  $(n - 1)$ -dimensional faces of the cones of  $\mathcal{T}_1$ ). Therefore, any zero-separating surface for  $\mathcal{T}_2$  will also be a zero-separating surface for  $\mathcal{T}_1$ .

**Remark 4.2.** *Similarly, it is also sufficient to focus on toric differential inclusions generated by a set of hyperplanes  $\mathcal{H}$  such that the  $\text{span}(\mathcal{L}) = \mathbb{R}^n$ , where  $\mathcal{L}$  is the set of orthogonal lines for the hyperplanes in  $\mathcal{H}$ . Indeed, if a toric differential inclusion  $\mathcal{T}$  has  $\text{span}(\mathcal{L}) \neq \mathbb{R}^n$ , then we can add to the set  $\mathcal{H}$  one or more hyperplanes to obtain  $\tilde{\mathcal{H}}$  such that  $\text{span}(\tilde{\mathcal{L}}) = \mathbb{R}^n$ . Now notice that the cone  $\tilde{F}(x)$  of the new toric differential inclusion  $\tilde{\mathcal{T}}$  contains the cone  $F(x)$  of the old toric differential inclusion  $\mathcal{T}$ , for all  $x \in \mathbb{R}_+^n$ . The inclusion relationship between the cones is due to the fact that all generators of a cone of  $\mathcal{T}$  are contained among the generators of a corresponding cone of  $\tilde{\mathcal{T}}$  (actually, the old cones are exactly the intersections between the new cones and the space  $\text{span}(\mathcal{L})$ ). Therefore  $\mathcal{T}$  is embedded in  $\tilde{\mathcal{T}}$ .*

## 4.1 One-dimensional toric differential inclusions

Consider a toric differential inclusion denoted  $\mathcal{T}_1$  in  $\mathbb{R}_+$ . Then, close enough to the origin,  $\mathcal{T}_1$  is simply the differential inclusion  $\frac{dx}{dt} \geq 0$ . In this case a zero-separating surface is just a point  $P_0 \in \mathbb{R}_+$  such that the cone of  $\mathcal{T}_1$  at  $P_0$  points away from zero. But, any point in  $\mathbb{R}_+$  that is close enough to zero has this property.

## 4.2 Two-dimensional toric differential inclusions

Consider a toric differential inclusion denoted  $\mathcal{T}_2$  in  $\mathbb{R}_+^2$ . Then, without loss of generality we can assume that  $\mathcal{T}_2$  is determined by a set of half-lines that start at the origin and bound cones in  $\mathbb{R}^2$  that can be used to generate  $\mathcal{T}_2$ . More exactly, for each such cone  $C$  its exponential image  $\text{exp}(C)$  is a subset<sup>25</sup> of  $\mathbb{R}_+^2$  where  $\mathcal{T}_2$  is constant and equal to the polar cone  $C^\circ$ , except near the boundary of  $\text{exp}(C)$ , where, far enough from the point  $(1, 1)$   $\mathcal{T}_2$  is a half-space, and near the point  $(1, 1)$   $\mathcal{T}_2$  is the whole space  $\mathbb{R}^2$ . Note that (as we can see in Fig. 2) in the construction of a zero-separating surface for  $\mathcal{T}_2$  only the half-lines contained in the 3rd quadrant of  $\mathbb{R}^2$  will really play a role.

There are many different ways to construct a zero-separating surface (which in this case is a zero-separating *curve*) for  $\mathcal{T}_2$ . The simplest way

---

<sup>25</sup> we will refer to such as set  $\text{exp}(C)$  as an *exp-cone* of  $\mathcal{T}_2$ .

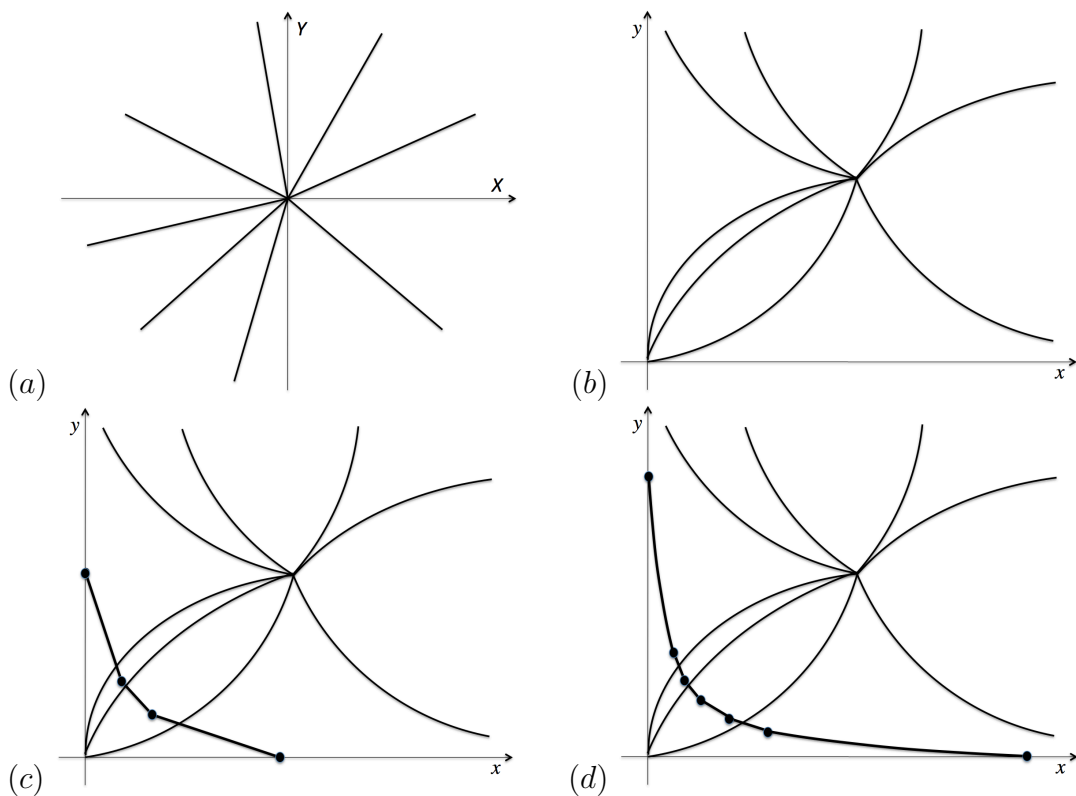


Figure 2: A polyhedral fan in  $\mathbb{R}^2$  (a) gives rise to a toric differential inclusion in  $\mathbb{R}_+^2$  (b). Neighborhoods of the curves shown in (b) delimit the uncertainty regions of the toric differential inclusion. We do not see these neighborhoods in (b), but we should imagine that each curve in (b) has some nonzero thickness that represents its uncertainty region, and the cone of the toric differential inclusion within that uncertainty region is a half-plane (each such half-plane is the polar cone of a half-line in (a)). This imposes that the zero-separating curve shown in (c) crosses these curves along line segments of specified slope; for each crossing of a curve in (c) the line segment must be orthogonal to the corresponding half-line in the 3rd quadrant of (a). In (d) we see that we may change the slope of the zero-separating curve outside the uncertainty regions. This is needed in order to obtain a faithful zero-separating curve. See also Section 3 in [1] for related examples discussed in more detail.

is to construct a polygonal line that connects a point on the  $x$ -axis to a point on the  $y$ -axis, in such a way that there exists exactly one polygonal vertex within each bounded exp-cone of  $\mathcal{T}_2$ , and the direction of each line segment follows the attracting direction of the (single) *uncertainly region* that it intersects (see Fig. 2(c)).

The construction described above is essentially the same as the construction of an invariant region in [1], but without having to continue the polygonal line all around the point (1,1) to obtain an invariant polygon.

On the other hand, note that we could have built the polygonal line above by using less stringent requirements on its line segments. For example, it is not necessary that each line segment follows the attracting direction of some uncertainly region; as long as this property is satisfied *within* that uncertainty region, then in all other regions we can have several line segments in various directions, as long as each one of them is a support line of the (locally constant) cone of  $\mathcal{T}_2$  in that region. Moreover, the zero-separating curve does not have to be a polygonal line; it can also contain arcs with nonzero curvature, as long as they are connected by straight line segments when crossing uncertainty regions (see Fig. 2(d)).

Note also that we can assume that the zero-separating curve constructed as above has the following additional property: within each bounded exp-cone of  $\mathcal{T}_2$ , the *slope* of the tangent line to the curve at points outside uncertainty regions belongs to the *interior* of the interval bounded by the slopes of the attracting directions of the uncertainty regions. We will say that such a curve is a *faithful zero-separating curve*. This special type of zero-separating curve will be used in the next section.

Note that since we can prove, as above, that two-dimensional toric differential inclusions in  $\mathbb{R}_+^2$  admit an exhaustive set of zero-separating curves, we obtain a proof of the general three-dimensional global attractor conjecture. This was first proved in [1], but the construction there is significantly more complex. On the other hand, no proof of the general four-dimensional global attractor conjecture has been found before, since for that we would need an exhaustive set of zero-separating surfaces for three-dimensional toric differential inclusions in  $\mathbb{R}_+^3$ . This is the topic of the next section.

### 4.3 Three-dimensional toric differential inclusions

Consider a toric differential inclusion denoted  $\mathcal{T}_3$  in  $\mathbb{R}_+^3$ . Then, without loss of generality we can assume that  $\mathcal{T}_3$  is generated by a set of planes  $\mathcal{H}_3$  such



that the set of lines  $\mathcal{L}_3$  that are orthogonal on the planes in  $\mathcal{H}_3$  satisfies  $\text{span}(\mathcal{L}_3) = \mathbb{R}^3$ .

We will also assume that for any line  $l \in \mathcal{L}_3$ , the lines that can be obtained from  $l$  by linear transformations given by permutations of the coordinate axes are also contained in  $\mathcal{L}_3$  (there are  $3! = 6$  such lines). In other words, we assume that  $\mathcal{L}_3$  is symmetric with respect to linear transformations given by permutations of the coordinate axes.

Moreover, we will also assume that the three coordinate axes are contained in  $\mathcal{L}_3$ , and the lines of the form  $\{x = 0, y = z\}$ ,  $\{y = 0, z = x\}$ ,  $\{z = 0, y = x\}$ , are also contained in  $\mathcal{L}_3$ .

It is difficult to represent the toric differential inclusion  $\mathcal{T}_3$  geometrically in  $\mathbb{R}^3$ , since we would have to draw many planes and all their intersections along lines. To simplify our figures, we will represent  $\mathcal{T}_3$  geometrically in  $\mathbb{R}^2$ , as described below.

In general, it is easier to describe the associated polar differential inclusion,  $\text{polar}(\mathcal{T}_3)$ , instead of  $\mathcal{T}_3$  itself. Since the connection between  $\mathcal{T}_3$  and  $\text{polar}(\mathcal{T}_3)$  is a simple logarithmic diffeomorphism (7) we will often describe  $\mathcal{T}_3$  using  $\text{polar}(\mathcal{T}_3)$ , and will refer to the domain  $\mathbb{R}^3$  of  $\text{polar}(\mathcal{T}_3)$  as *logarithmic space*.

Since the information about  $\mathcal{T}_3$  is contained in the set  $\mathcal{H}_3$  of planes that bound the regions on which  $\text{polar}(\mathcal{T}_3)$  is constant, we describe a way to visualize these planes in  $\mathbb{R}^2$ . Note also that only the planes that intersect the negative orthant are of interest for the construction of a zero-separating surface<sup>26</sup>. Moreover, all these planes contain the origin, so they are in one-to-one correspondence with lines in the plane  $X + Y + Z = -1$  that intersect the triangle  $\{X + Y + Z = -1\} \cap \mathbb{R}_-^3$ .

Moreover, due to the permutation symmetries mentioned above, it is sufficient if we construct a zero-separating surface only in one of the 6 regions given by specifying inequalities between  $x$ ,  $y$  and  $z$ , for example in the region  $\{x \leq y \leq z\} \cap \mathbb{R}_+^3$ , which is shaded in Fig. 3. If we map this region to logarithmic space we obtain the region  $\{X \leq Y \leq Z\} \subset \mathbb{R}^3$ , which, when intersected with the triangle  $\{X + Y + Z = -1\} \cap \mathbb{R}_-^3$ , gives us a smaller triangle, similar to the one shaded in Fig. 3 (except that it is in the negative orthant).

Further, we map this smaller triangle (given by  $\{X \leq Y \leq Z\} \cap \{X + Y +$

---

<sup>26</sup> similarly, in the previous section, only the lines that intersected the 3rd quadrant were relevant to our construction of a zero-separating curve.

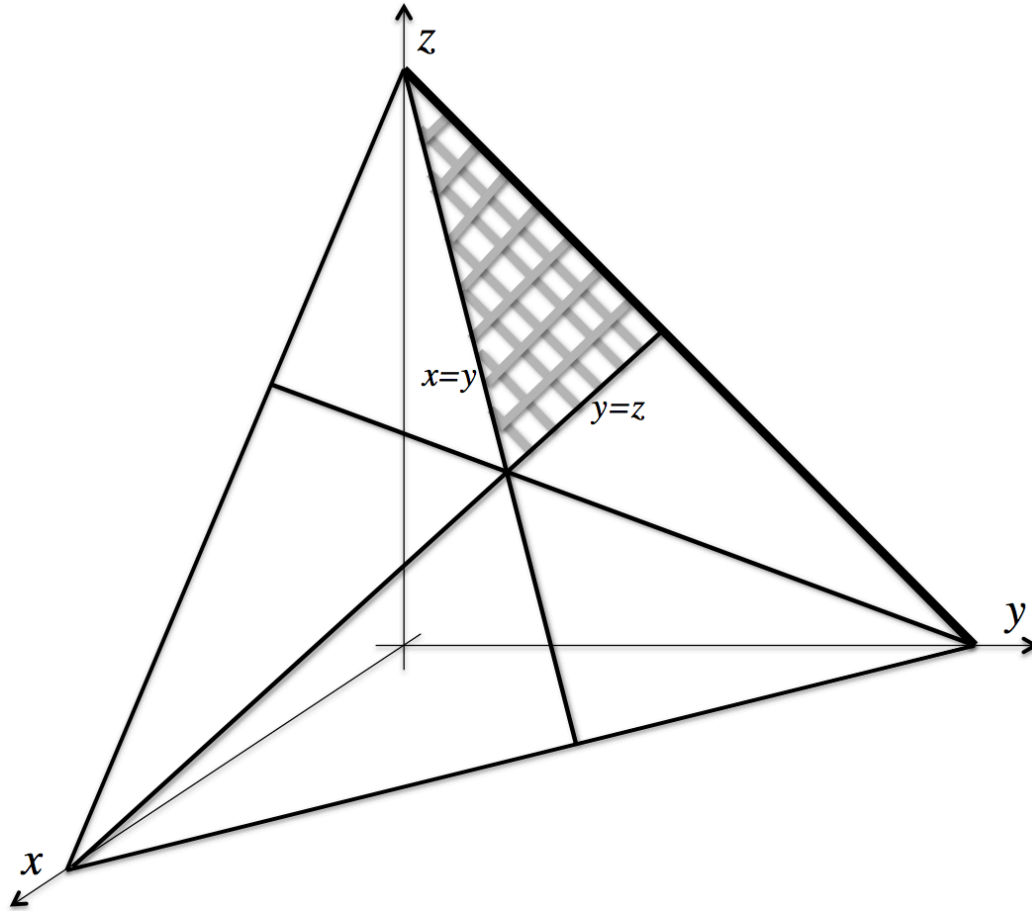


Figure 3: We partition the domain  $\mathbb{R}_+^3$  into six regions that are mapped into each-other by the six symmetries given by permutations of the axes. The shaded triangle points out the region  $\mathcal{R}_3 = \{(x, y, z) \in \mathbb{R}_+^3 \mid x \leq y \leq z\}$ .

$Z = -1\} \cap \mathbb{R}_-^3$ ) to the plane  $\{Z = 1\}$  by dividing<sup>27</sup> all the coordinates by  $Z$ . This transformation can be regarded geometrically as follows: we consider the line through a point  $(X, Y, Z)$  and the origin; then we map this point to the intersection between this line and the plane  $\{Z = 1\}$ . In particular, it follows that line segments inside the domain  $\{X \leq Y \leq Z\} \cap \{X + Y + Z = -1\} \cap \mathbb{R}_-^3$  are mapped to line segments inside the plane  $\{Z = 1\}$ ; moreover, the image

<sup>27</sup> we can regard the new coordinates in the plane  $\{Z = 1\}$  are projective coordinates.

of this mapping is  $\{X \geq Y \geq Z\} \cap \{Z = 1\} \subset \mathbb{R}_+^3$ , and can also be written as  $\{(X, Y, 1) \in \mathbb{R}^3 \mid X \geq Y \geq 1\}$ .

Note now that each plane that intersects the region  $\{X \leq Y \leq Z\}$  of the negative orthant can be represented uniquely by a line segment within the triangle  $\{X \leq Y \leq Z\} \cap \{X + Y + Z = -1\} \cap \mathbb{R}_-^3$  (such that the endpoints of the line segment are on the edges of the triangle), which in turn can be represented uniquely by a line segment or a half-line within the “unbounded triangle”  $\{(X, Y, 1) \in \mathbb{R}^3 \mid X \geq Y \geq 1\}$ . The endpoints of these segments or half-lines are on the edges of the unbounded triangle.

Moreover, we can map the set  $\{(X, Y, 1) \in \mathbb{R}^3 \mid X \geq Y \geq 1\}$  to  $\mathbb{R}^2$  by simply projecting on the  $XY$ -plane. Then the toric differential inclusion  $\mathcal{T}_3$  can be represented by a set of line segments and half-lines in the region  $\{(X, Y) \in \mathbb{R}^2 \mid X \geq Y \geq 1\}$ , as shown in Fig. 4(a). (We do not need to consider all 6 such regions since we have assumed that  $\mathcal{L}_3$  is symmetric with respect to linear transformations given by permutations of the coordinate axes.)

Note that, without loss of generality, we can assume that  $\mathcal{T}_3$  also contains additional horizontal half-lines through all the intersection points of line segments and half-lines in Fig. 4(b), and additional non-horizontal line segments connecting these intersection points, such that all the regions bounded by line segments are simplicial (i.e., triangular), as shown in Fig. 4(c). In particular, this means that we now no longer regard  $\mathcal{T}_3$  as a *hyperplane-generated* toric differential inclusion, but it is now a *general* toric differential inclusion.

We consider now the set  $\mathcal{D}_2 = \{(X, Y) \in \mathbb{R}^2 \mid X \geq Y \geq 1\}$  and its simplicial partition with line segments and half-lines described above and in Fig. 4. Consider also the set  $\mathcal{R}_3 = \{(x, y, z) \in \mathbb{R}_+^3 \mid x \leq y \leq z\}$ . We will construct a function  $\varphi : \mathcal{D}_2 \rightarrow \mathcal{R}_3$  whose graph (together with its symmetric images with respect to permutations of axes) will form a zero-separating surface for  $\mathcal{T}_3$ .

Consider a *faithful* zero-separating curve (obtained as described in the previous section) along the half line  $\{(X, Y) \in \mathbb{R}^2 \mid X = Y \geq 1\}$  in  $\mathcal{D}_2$ , which is the left-side boundary of  $\mathcal{D}_2$  in Fig. 5. Consider the partition of the domain  $\mathcal{D}_2$  shown in Fig. 5. This partition was obtained as follows.

The shaded stripes start on the left side at the points given by the zero-separating curve mentioned above, and go approximately horizontally across, as shown. We will see later how exactly we choose the upper and lower boundaries of the shaded stripe regions. Along each shaded stripe region there are vertical line segments in between each pair of consecutive simplicial parti-

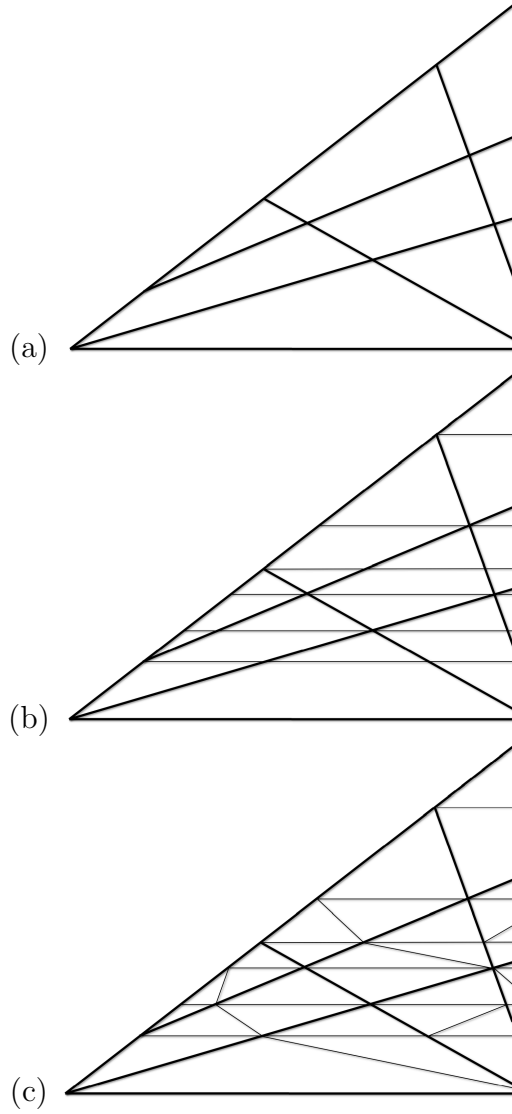


Figure 4: We partition the domain  $\mathcal{D}_2$  into triangles, in several stages: (a) To begin with, the domain  $\mathcal{D}_2$  is crossed by lines that represent the planes of the hyperplane-generated  $\text{polar}(\mathcal{T}_3)$ . Then, in (b) we draw additional horizontal lines through all the intersection points of lines in (a). Finally, in (c) we draw additional non-horizontal line segments to subdivide each polygon in (b) into triangles, without adding additional intersection points.

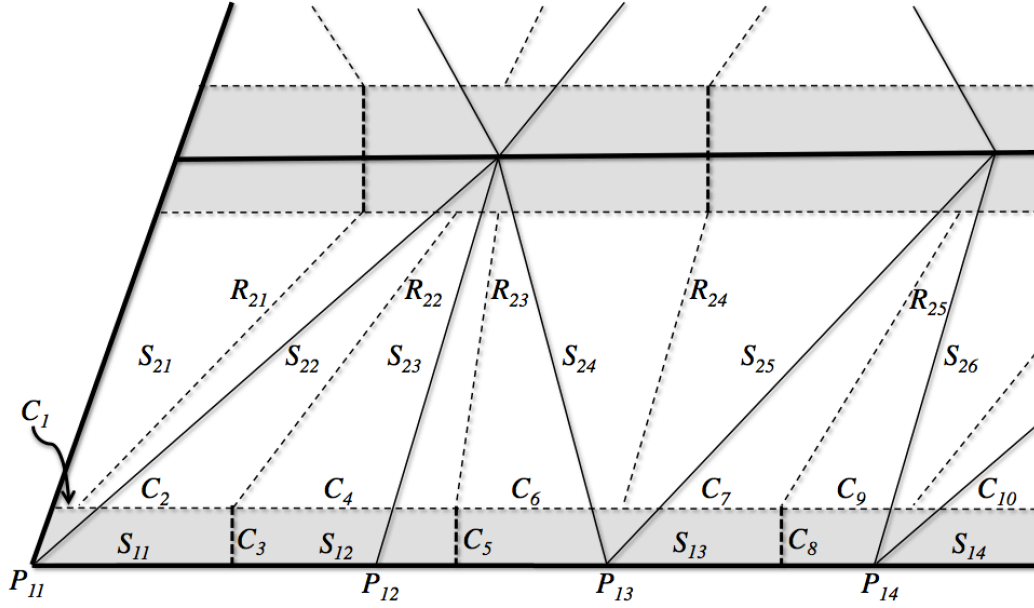


Figure 5: *This diagram represents a further partition of  $\mathcal{D}_2$  into regions. Our construction of the map  $\varphi$  (whose graph is a zero-separating surface for  $\mathcal{T}_3$ ) uses this diagram to proceed from one region to the next, as explained below. Regions are denoted  $\mathcal{S}_{ij}$ , and the curves  $C_i$  and  $R_{ij}$  represent boundaries between regions. Each region  $\mathcal{S}_{1j}$  contains exactly one point where two or more solid lines intersect, denoted  $P_{1j}$ .*

tion vertices, and these vertical line segments connect a point on the lower boundary of the shaded stripe with another point on the upper boundary of the shaded stripe, as shown in Fig. 5. Also, there is exactly one dotted line segment within each region of the simplicial partition, and it connects an upper boundary point on the lower shaded stripe with a lower boundary point on the upper shaded stripe, as shown in Fig. 5.

We now describe in more detail how this partition is generated, and how it allows us to construct the function  $\varphi : \mathcal{D}_2 \rightarrow \mathcal{R}_3 = \{(x, y, z) \in \mathbb{R}_+^3 \mid x \leq y \leq z\}$  mentioned above.

Note that the union of curves  $\bigcup_{(X,Y) \in \mathcal{D}_2} \{(t^X, t^Y, t) \mid t > 0\}$  forms a disjoint partition of the set  $\mathcal{R}_3$  near the origin, and any zero-separating surface close

enough to the origin must contain a point on each one of the curves in the union above.

We will think of each point  $(X, Y) \in \mathcal{D}_2$  as associated to the curve  $\{(t^X, t^Y, t) \mid t > 0\}$ , and we will define the function  $\varphi$  such that  $\varphi(X, Y)$  lies on this curve. In other words, consider the function  $\psi : \mathcal{R}_3 \cap B_\varepsilon \rightarrow \mathcal{D}_2$  such that for each point  $(x, y, z) \in \mathcal{R}_3$  at distance at most  $\varepsilon$  to the origin we have that  $\psi(x, y, z) = (X, Y) \in \mathcal{D}_2$  such that there exists some  $t > 0$  with  $(x, y, z) = (t^X, t^Y, t)$ . (Note that actually  $t = z$ .) Then, we will define the function  $\varphi$  such that  $\psi \circ \varphi : \mathcal{D}_2 \rightarrow \mathcal{D}_2$  is the identity function.

This means that if we specify a point  $(x_0, y_0, z_0) \in \mathcal{R}_3$  which is on the graph of the function  $\varphi$ , then we have also implicitly specified exactly for which point  $(X_0, Y_0) \in \mathcal{D}_2$  we have  $\varphi(X_0, Y_0) = (x_0, y_0, z_0)$ . So, to define the function  $\varphi$ , it is enough to specify the surface  $\mathcal{S}_\varphi$  in  $\mathcal{R}_3$  which is the graph of  $\varphi$ .

As we mentioned above, we start by defining the graph of  $\varphi$  along the left-side boundary of  $\mathcal{D}_2$ , i.e., along the half-line  $\{(X, Y) \in \mathbb{R}^2 \mid X = Y \geq 1\}$ , and we do so by using a faithful two-dimensional zero-separating surface (i.e., curve) along this half-line, constructed as described in the previous section. This gives us a left-side boundary for the surface  $\mathcal{S}_\varphi$  (if we think of the surface  $\mathcal{S}_\varphi$  as lying in Fig. 3, where the plane  $\{x = y\}$  is to the left of the region  $\mathcal{R}_3$ ).

In particular, we choose the flat regions of the left-side boundary of  $\mathcal{S}_\varphi$  to be short enough, so the shaded regions are thin enough to allow the vertical lines shown in each shaded region to cross that shaded region without intersecting other lines (we may have to move the construction closer to the origin to make this possible)<sup>28</sup>.

We now explain how we define  $\varphi$  on the various patches of  $\mathcal{D}_2$  shown in Fig. 5, and, equivalently, we construct patches of the surface  $\mathcal{S}_\varphi$  in  $\mathcal{R}_3$  such that when we map each such patch to  $\mathcal{D}_2$  via  $\psi$ , we obtain one of the patches of  $\mathcal{D}_2$  shown in Fig. 5.

The left-bottom patch of  $\mathcal{S}_\varphi$  is flat, given by a plane whose normal vector is  $(P_{11}, 1) = (1, 1, 1)$ , where the point  $P_{11}$  is the corner of the domain  $\mathcal{D}_2$ . Note that this flat patch  $\mathcal{S}_{11}$  is compatible with the zero-separating curve on the left-side boundary of  $\mathcal{S}_\varphi$ .

---

<sup>28</sup>We plan to construct a zero-separating surface based on the “blueprint” shown in Fig. 5. The blueprint comes with a specified width for the shaded horizontal stripes, to accommodate other features, as we will see later. We don’t need to change this blueprint to accommodate a larger value of  $\delta$ ; instead, we can compensate for the larger  $\delta$  just by moving the whole construction of the zero-separating surface closer to the origin.

The boundary of this patch is made up of line segments, and we describe them as follows. Note how in Fig. 5 the boundary of the image of this patch in  $\mathcal{D}_2$  consists of three curves, denoted  $C_1, C_2, C_3$ . Each one of these curves intersects exactly one solid line segment, and recall that the solid line segments in Fig. 5 represent the *separating surfaces*<sup>29</sup> of  $\mathcal{T}_3$ . To simplify the terminology we will say that to each black line segment in Fig. 5 there corresponds an *attracting direction*<sup>30</sup> of  $\mathcal{T}_3$ .

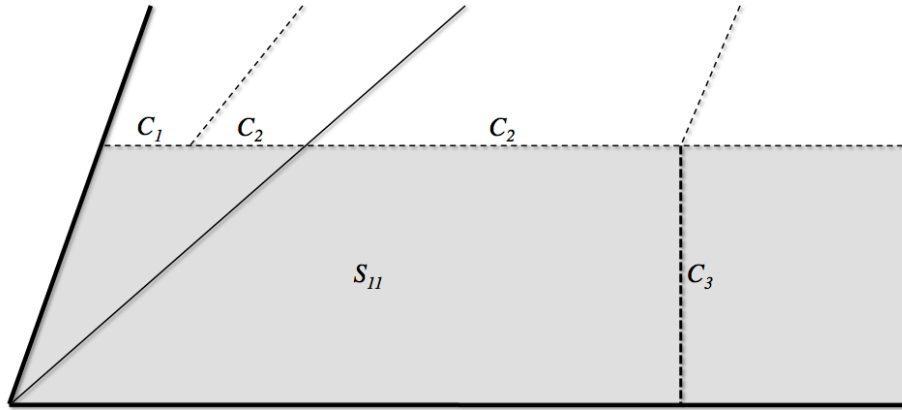


Figure 6: *Zoom in on the left-side corner of the diagram in Fig. 5.*

Then, we choose  $C_1$  such that the boundary  $\varphi(C_1)$  of the flat patch  $\mathcal{S}_{11}$  is a line segment in the attracting direction of the black line segment that  $C_1$  intersects, and we choose  $C_2$  and  $C_3$  similarly. Since each one of  $\varphi(C_1), \varphi(C_2), \varphi(C_3)$  is orthogonal to a plane that contains the line corresponding to the point  $(P_{11}, 1)$ , it follows that they do indeed belong to a common plane, which is orthogonal to the vector  $(P_{11}, 1)$ .

Note that, since  $\varphi(C_3)$  is a line segment in the attracting direction of a *horizontal* segment in Fig. 5, it follows that the  $x$ -coordinates of points along  $\varphi(C_3)$  must be constant; therefore the  $X$ -coordinates of points along  $C_3$  must also be constant, because  $C_3 = \psi(\varphi(C_3))$ . Therefore,  $C_3$  is flat and orthogonal on the horizontal black line segment it intersects.

<sup>29</sup>the *separating surfaces* of  $\mathcal{T}_3$  are exponential images of the hyperplanes that generate  $\text{polar}(\mathcal{T}_3)$ .

<sup>30</sup>As we discussed before, the *attracting directions* are easier to describe for  $\text{polar}(\mathcal{T}_3)$ ; but recall that if we take into account the correspondence between their separating surfaces, then  $\mathcal{T}_3$  and  $\text{polar}(\mathcal{T}_3)$  have the same attracting directions.

On the other hand,  $\varphi(C_2)$  is a line segment in the attracting direction of a *non-horizontal* segment in Fig. 5, so the  $x$ -coordinates along  $\varphi(C_2)$  are *not* constant. This means that  $C_2$  is *not* perfectly horizontal, although it may appear so in Fig. 5 and Fig. 6. But, when we map  $\varphi(C_2)$  through  $\psi$  to obtain  $C_2$ , the image must be a curve with *almost horizontal* tangent line. We can see this by checking that, if we fix some values  $X > Y > 1$  and  $0 < t \ll 1$  and we calculate the Jacobian of  $\psi$  at the point  $(t^X, t^Y, t)$ , we obtain the matrix

$$\frac{\log t}{t} \begin{pmatrix} t^{1-X} & 0 & -X \\ 0 & t^{1-Y} & -Y \end{pmatrix}. \quad (10)$$

Note now that, given the assumptions above we have  $t^{1-X} \gg X$  and  $t^{1-Y} \gg Y$ , and also  $t^{1-X} \gg t^{1-Y}$ . This explains why  $C_2$  is approximately horizontal everywhere. The case of  $C_1$  is similar, except that  $C_1$  reaches the line  $\{X = Y\}$  in  $\mathcal{D}_2$ , so  $C_1$  is approximately horizontal far enough from that line, while close enough to the line  $\{X = Y\}$  the curve  $C_1$  becomes approximately orthogonal to it.

Let us look now at the second shaded patch  $\mathcal{S}_{12}$  on the bottom shaded stripe, such that  $\psi(\mathcal{S}_{12})$  is bounded by the curves  $C_3, C_4$  and  $C_5$  in Fig. 5. This will also be a flat patch, given by a plane whose normal vector is  $(P_{12}, 1)$ , where  $P_{12}$  is the intersection point of solid lines within the patch  $\mathcal{S}_{12}$ .

Note first that the patch  $\mathcal{S}_{12}$  is compatible with the patch  $\mathcal{S}_{11}$  we constructed before, because they meet along the line segment  $\varphi(C_3)$ , and, since  $\varphi(C_3)$  is orthogonal to the plane in  $\mathbb{R}^3$  determined by the horizontal black line it intersects, it follows that it is also orthogonal to any line within this plane, and in particular it is orthogonal to the vectors  $(P_{11}, 1)$  and  $(P_{12}, 1)$ . Therefore the patch  $\mathcal{S}_{12}$  is compatible with the patch  $\mathcal{S}_{11}$ , i.e., they intersect along the line segment  $\varphi(C_3)$  whose direction is indeed the intersection of the two planes that give  $\mathcal{S}_{11}$  and  $\mathcal{S}_{12}$ .

The construction of  $C_4$  is similar to the construction of  $C_2$ , and the construction of  $C_5$  is similar to the construction of  $C_3$ .

After this, the construction of the other patches  $\mathcal{S}_{1j}$  in the on the bottom shaded stripe of Fig. 5 proceeds similarly. We will now discuss the construction of the patches along the bottom white stripe of Fig. 5. Let us start by looking at the patch denoted  $\mathcal{S}_{21}$ .

As before, we start with a zero-separating curve along the left-side boundary of this patch. Starting from each point of this curve, we draw a line segment in the attracting direction of the left-side boundary line, and con-



tinue it to the right until it reaches the surface represented by the dotted line segment  $R_{21}$  in Fig. 5. We obtain a curve along the surface represented by  $R_{21}$ , and then, starting from each point of this curve, we draw a line segment in the attracting direction of the next black boundary line, and continue it to the right until it reaches the surface represented by the dotted line segment  $R_{22}$  in Fig. 5. This will give us a curve along the surface represented by  $R_{22}$ , and we continue the construction in the same way until we fill in this bottom white stripe of Fig. 5 completely.

Next, we construct the zero-separating surface  $\varphi(\mathcal{D}_2)$  along the second shaded stripe of Fig. 5, then the second white stripe, and so on. Along each stripe the construction starts on the left-hand side of the domain  $\mathcal{D}_2$  and, one by one, fills in each region in the partition shown in Fig. 5.

We need now to check that  $\varphi(\mathcal{D}_2)$  (together with its 6 symmetric images) is indeed a zero-separating surface for  $\mathcal{T}_3$ . For this it is enough to see that, within each region in the partition shown in Fig. 5, the surface  $\varphi(\mathcal{D}_2)$  is a support surface of the cone of  $\mathcal{T}_3$  in that region.

First we check that  $\varphi(\mathcal{D}_2)$  satisfies the conditions necessary for being a zero-separating surface for  $\mathcal{T}_3$  along the shaded region patches. Indeed, all the surface patches of  $\varphi(\mathcal{D}_2)$  in the shaded regions of  $\mathcal{D}_2$  are flat plane patches, and for each shaded patch that plane is exactly the cone of  $\mathcal{T}_3$  at the black point that lies at the center of that patch, so it follows that  $\varphi(\mathcal{D}_2)$  is a support surface of the cone of  $\mathcal{T}_3$  in all shaded regions in Fig. 5.

Consider now the first white patch we constructed, denoted  $\mathcal{S}_{21}$ . We will argue that the tangent plane at any point of this patch is a support plane of the cone of  $\mathcal{T}_3$  in that leftmost lower triangle of the partition in Fig. 5. Recall that the left half of  $\mathcal{S}_{21}$  (up to the surface represented by  $R_{21}$ ) was constructed as a *ruled surface* that started from the left-side boundary curve  $C_0$ , which was part of a faithful zero-separating curve along the line  $\{X = Y\}$ . The direction of the straight line segments along this ruled surface was the attracting direction of the surface represented by  $R_{21}$ . Then the tangent plane to this ruled surface must contain this constant attracting direction.

If we imagine the construction above for the case where the left-side boundary curve  $C_0$  is replaced by a short line segment  $l_0$  within the plane  $\{x = y\}$ , then the ruled surface is a plane patch  $\pi_0$ . Then note that the normal to  $\pi_0$  is the same as the normal to  $l_0$  within the plane  $\{x = y\}$ , because  $\pi_0$  is orthogonal to  $\{x = y\}$ <sup>31</sup>. Therefore, by approximating  $C_0$  with

---

<sup>31</sup>In general, if we have a codimension-two linear subspace  $l$  contained in a hyperplane

polygonal lines and then taking the limit, we obtain that the normal to  $\mathcal{S}_{21}$  at a point  $\varphi(P)$  is approximately the same as the normal to  $C_0$  within the plane  $\{x = y\}$ , calculated at a point  $P_0$  which is obtained by drawing a horizontal line from  $P$  and intersecting it with the line  $\{X = Y\}$  in Fig. 5 (here we are using the fact that the image via  $\psi$  of a line segment that passes through  $\varphi(P)$  and is orthogonal on  $\{x = y\}$  is approximately the horizontal line from  $P$  to the line  $\{X = Y\}$ ). Then we obtain that the surface patch  $\mathcal{S}_{21}$  does satisfy the condition that its outer normal vector belongs to the cone corresponding to the region  $\psi(\mathcal{S}_{21})$  in  $\mathcal{D}_2$ , so  $\mathcal{S}_{21}$  is a *zero-separating surface patch*<sup>32</sup> for  $\mathcal{T}_3$ .

Consider now the second white patch we constructed, denoted  $\mathcal{S}_{22}$  in Fig. 5. The surface represented by  $R_{21}$  is asymptotically close to the plane  $\{x = 0\}$  in  $\mathbb{R}^3$  (i.e., if the neighborhood of the origin in  $V_0 \subset \mathbb{R}^3$  is small enough then this surface is arbitrarily close even in relative terms).<sup>33</sup>

Then, consider a polygonal line approximation of the right-side boundary curve of  $\mathcal{S}_{21}$ , such that each line segment in this polygonal line is approximately parallel to the plane  $\{x = 0\}$ . Denote one such polygonal line segment by  $l_1$ . If we construct a plane starting from  $l_1$  and going in the attracting direction of the surface represented by the solid line in region  $S_{22}$  in Fig. 5, then the normal to this plane will have to lie on the plane represented by the solid line and also will have to be contained in the dihedral angle represented by the white stripe (because it has to be orthogonal both to the

---

$\mathcal{H}$ , and we build a hyperplane  $\pi$  by extending from  $l$  in a direction orthogonal to  $\mathcal{H}$ , then the normal line to  $l$  within  $\mathcal{H}$  is the same as the normal line of the hyperplane  $\pi$ . (This will be useful for higher dimensional constructions similar to the one above, with  $l$  inside the hyperplane  $\mathcal{H} = \{x = y\}$  in  $\mathbb{R}^n$ .)

<sup>32</sup> i.e., it is a surface patch that has the local properties of a zero-separating surface for  $\mathcal{T}_3$ .

<sup>33</sup> Consider a surface  $z = x^\alpha y^\beta$  that contains the curve  $\{(t^{\gamma_1}, t^{\gamma_2}, t) | t > 0\}$  for some  $\gamma_1 > \gamma_2 > 1$ . The normal to the surface is given by  $\text{grad}(x^\alpha y^\beta - z) = (\alpha x^{\alpha-1} y^\beta, \beta x^\alpha y^{\beta-1}, -1)$ , so the normal at a point  $(t_0^{\gamma_1}, t_0^{\gamma_2}, t_0)$  is given by the vector  $(\alpha t_0^{(\alpha-1)\gamma_1 + \beta\gamma_2}, \beta t_0^{\alpha\gamma_1 + (\beta-1)\gamma_2}, -1) = (\alpha t_0^{1-\gamma_1}, \beta t_0^{1-\gamma_2}, -1)$ , because  $\alpha\gamma_1 + \beta\gamma_2 = 1$ . If  $t_0$  is small enough then  $t_0^{1-\gamma_1} \gg t_0^{1-\gamma_2} \gg 1$ . Therefore, if  $\alpha \neq 0$ , the normal vector  $(\alpha t_0^{1-\gamma_1}, \beta t_0^{1-\gamma_2}, -1)$  is approximately along the  $x$ -axis.

This calculation does not include  $z$ -independent surfaces of this kind, i.e., surfaces of the form  $1 = x^\alpha y^\beta$  such that  $\alpha\gamma_1 + \beta\gamma_2 = 0$  for some  $\gamma_1 > \gamma_2 > 1$ . Note that the normal vector  $(\alpha t_0^{1-\gamma_1}, \beta t_0^{1-\gamma_2}, -1)$  is simply replaced by  $(\alpha t_0^{1-\gamma_1}, \beta t_0^{1-\gamma_2}, 0)$  in this case. Alternatively, we can analyze all cases at once by looking at the surface  $1 = x^\alpha y^\beta z^\gamma$  instead of the surface  $z = x^\alpha y^\beta$ ; then the normal at the point  $(t_0^{\delta_1}, t_0^{\delta_2}, t_0)$  becomes  $(\alpha t_0^{-\delta_1}, \beta t_0^{-\delta_2}, \gamma t_0^{-1})$ , and we still have  $t_0^{-\delta_1} \gg t_0^{-\delta_2} \gg t_0^{-1}$ .

attracting direction of the surface represented by the line  $C_8$ , and to the line segment by  $l_1$  we started with, and because the original zero-separating *curve* that gave us the left-side initial condition was *faithful*). Therefore the second white patch we construct (denoted by  $\mathcal{S}_{22}$  in Fig. 5) is also a zero-separating surface patch for  $\mathcal{T}_2$ .

We can now continue towards the right in the lowest white stripe in Fig. 5, and conclude that we have constructed a zero-separating surface patch for  $\mathcal{T}_2$  along this whole white stripe in  $\mathcal{D}_2$ . Then we do the same for the next higher shaded stripe, and then for the next higher white stripe, and so on. In conclusion, it follows that  $\varphi(\mathcal{D}_2)$  is a zero-separating surface for  $\mathcal{T}_2$ .

Note that the zero-separating surface  $\varphi(\mathcal{D}_2)$  we have constructed above is *not faithful*. We can obtain a faithful zero-separating surface  $\tilde{\varphi}(\mathcal{D}_2)$  by using a similar construction, but based on a partition of  $\mathcal{D}_2$  like the one shown in Fig. 10.

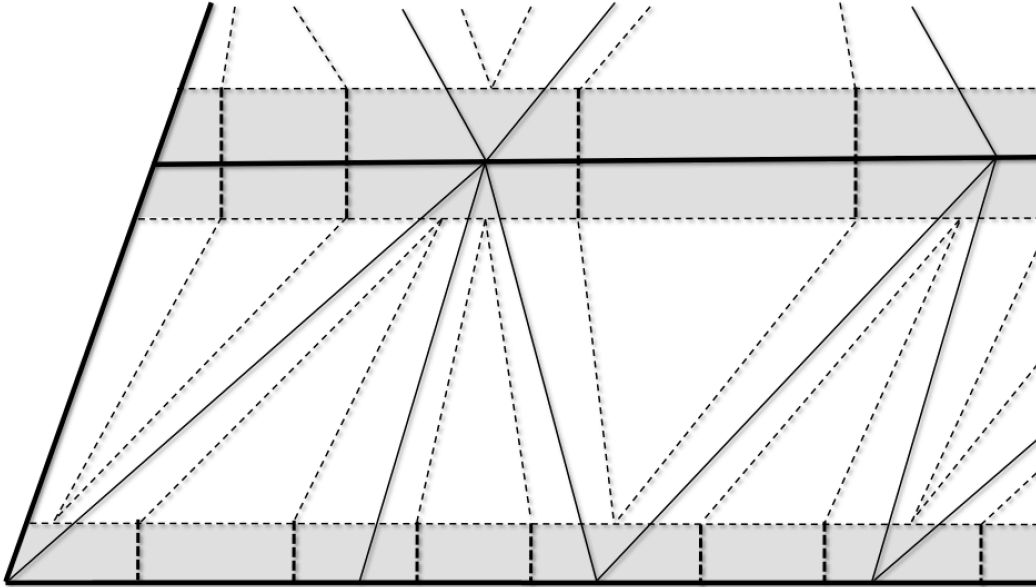


Figure 7: A *different partition of  $\mathcal{D}_2$ , that can be used to build a faithful zero-separating surface for  $\mathcal{T}_3$ .*

Note that each triangular patch in Fig. 10 is now divided into three sub-patches (and not just two as before). Of these three sub-patches, we define

$\tilde{\varphi}$  along the left-side and right-side patches as before, but for the middle sub-patch we proceed differently, to ensure that we obtain a faithful zero-separating surface.

For each middle sub-patch within a shaded stripe we define  $\tilde{\varphi}$  to be not linear along the horizontal direction (as before) but to vary along this direction in such a way that the normal to the graph of  $\tilde{\varphi}$  at a point  $\tilde{\varphi}(P)$  is very close to the projection of  $P$  on the black horizontal line along the patch. (This property can be ensured by first defining  $\tilde{\varphi}$  along the black line, and then extending the graph of  $\tilde{\varphi}$  to the middle sub-patch via line segments that are orthogonal to the black line.)

Also, for each middle sub-patch within a white stripe we define  $\tilde{\varphi}$  such that the normal to the graph of  $\tilde{\varphi}$  at a point  $\tilde{\varphi}(P)$  is very close to  $P$  itself. (One way to accomplish this is formulate this condition as a first order PDE with left-side boundary condition given by the already constructed graph of  $\tilde{\varphi}$  on the left side of the middle sub-patch.)

#### 4.4 Four-dimensional toric differential inclusions

Consider a toric differential inclusion denoted  $\mathcal{T}_4$  in  $\mathbb{R}_+^4$ . Without loss of generality (analogous with the previous section) we can assume that  $\mathcal{T}_4$  is generated by a set of hyperplanes  $\mathcal{H}_4$  with a set of orthogonal lines  $\mathcal{L}_4$  such that  $\text{span}(\mathcal{L}_4) = \mathbb{R}^4$ .

Also analogous with the previous section, we will assume that for any line  $l \in \mathcal{L}_4$ , the lines that can be obtained from  $l$  by linear transformations given by permutations of the coordinate axes are also contained in  $\mathcal{L}_4$  (there are  $4! = 24$  such lines). In other words, we assume that  $\mathcal{L}_4$  is symmetric with respect to linear transformations given by permutations of the coordinate axes.

Moreover, we will also assume that the three coordinate axes are contained in  $\mathcal{L}_4$ , and the lines of the form  $\{x = y, z = 0, w = 0\}$ ,  $\{x = z, y = 0, w = 0\}$ ,  $\{y = z, x = 0, w = 0\}$ ,  $\{x = w, y = 0, z = 0\}$ ,  $\{y = w, x = 0, z = 0\}$ ,  $\{z = w, x = 0, y = 0\}$  are also contained in  $\mathcal{L}_4$ .

It is difficult to represent the toric differential inclusion  $\mathcal{T}_4$  geometrically in  $\mathbb{R}^4$  in a useful way. To be able to draw some useful figures, we will represent key parts of  $\mathcal{T}_4$  geometrically in  $\mathbb{R}^3$ , as described below.

All the information about  $\mathcal{T}_4$  is contained in the set of hyperplanes that bound the cones of its associated polar differential inclusion,  $\text{polar}(\mathcal{T}_4)$ . Only

the hyperplanes that intersect the negative orthant are of interest for the construction of a zero-separating surface. Moreover, all these hyperplanes contain the origin, so they are in one-to-one correspondence with two-dimensional planes in the hyperplane  $X + Y + Z + W = -1$  that intersect the tetrahedron  $\{X + Y + Z + W = -1\} \cap \mathbb{R}_-^4$ .

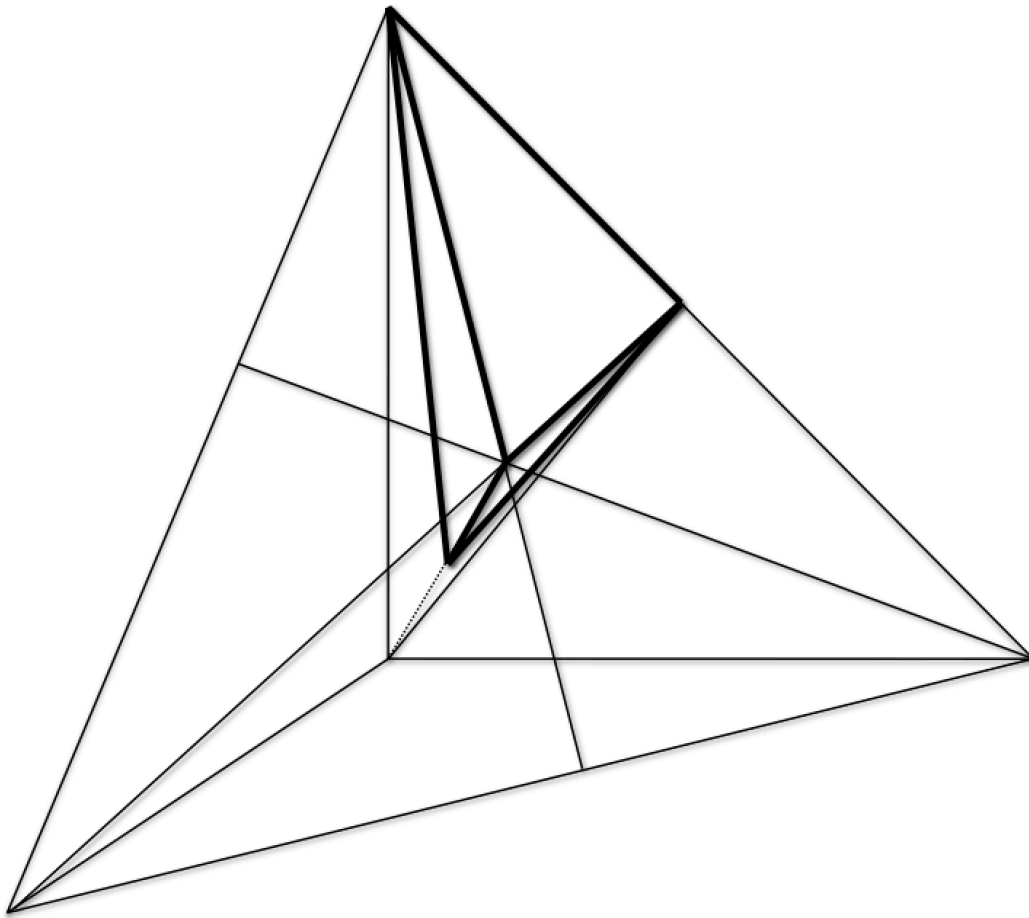


Figure 8: *Like in the previous section, we use the symmetries of  $\mathcal{T}_4$  to divide the problem into  $4!=24$  smaller problems. The domain  $\mathcal{D}_3$  is obtained by mapping into  $\mathbb{R}^3$  one of the 24 tetrahedra, such as the one with thick edges shown above.*

Moreover, due to the permutation symmetries mentioned above, it is

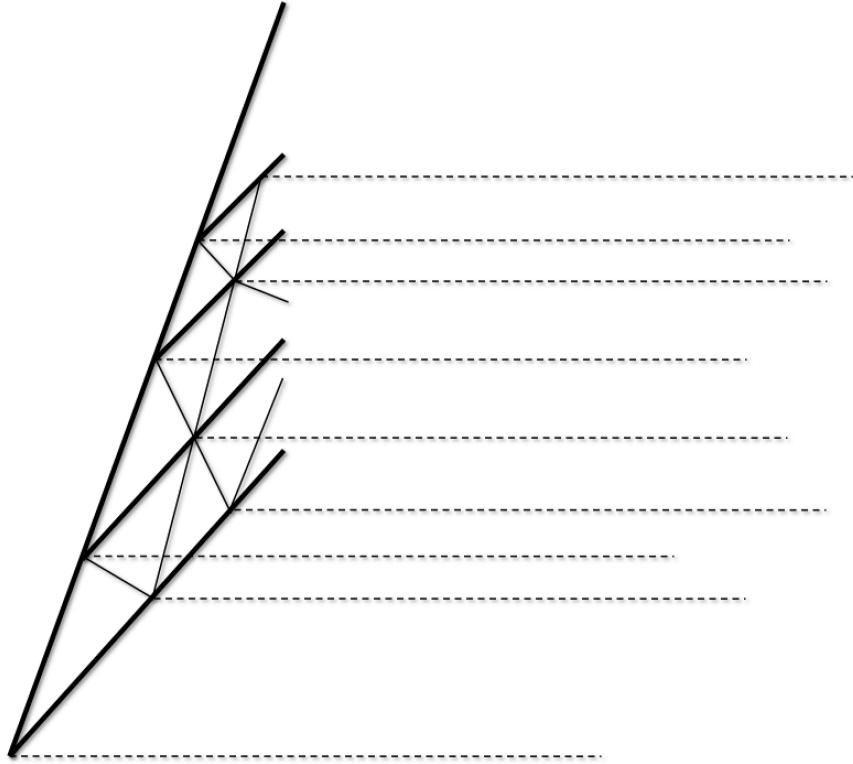


Figure 9: *The construction of the function  $\varphi$  in the previous section has proceeded one step at a time, first the bottom shaded layer of  $\mathcal{D}_2$ , then the bottom white layer, and so on. The analogous construction in this section features 3d “tunnels” instead of 2d layers, as shown above. In the figure above we should think of the configuration of solid lines as being all in the same plane, on the left-side facet of  $\mathcal{D}_3$ , and representing the domain of a left-side boundary condition for  $\varphi$ . Then, each solid line segment of the left-side facet of  $\mathcal{D}_3$  determines a (flat) surface patch inside  $\mathcal{D}_3$ , obtained by drawing lines in the  $X$ -direction that start on that line segment. The dotted lines shown above are lines of this kind that happen to pass through intersection points of two or more segments on the left-side facet of  $\mathcal{D}_3$ . These dotted lines and the flat surface patches that connect them determine the boundaries of the 3d tunnels we mentioned above. There is additional subdivision within these patches, as explained in Fig. 10.*

sufficient if we construct a zero-separating surface only in one of the 24 regions given by specifying inequalities between  $x$ ,  $y$ ,  $z$  and  $w$ , for example in the region  $\{x \leq y \leq z \leq w\} \cap \mathbb{R}_+^4$ . If we map this region to logarithmic space we obtain the region  $\{X \leq Y \leq Z \leq W\} \subset \mathbb{R}^4$ , which, when intersected with the tetrahedron  $\{X+Y+Z+W = -1\} \cap \mathbb{R}_-^4$ , gives us a smaller tetrahedron, similar to the situation shown in Fig. 8.

Further, we map this smaller tetrahedron (given by  $\{X \leq Y \leq Z \leq W\} \cap \{X+Y+Z+W = -1\} \cap \mathbb{R}_-^4$ ) to the plane  $\{W = 1\}$  by dividing all the coordinates by  $W$ . This transformation can be regarded geometrically as follows: we consider the line through a point  $(X, Y, Z, W)$  and the origin; then we map this point to intersection between this line and the hyperplane  $\{W = 1\}$ . In particular, it follows that line segments inside the domain  $\{X \leq Y \leq Z \leq W\} \cap \{X+Y+Z+W = -1\} \cap \mathbb{R}_-^4$  are mapped to line segments inside the plane  $\{W = 1\}$ ; moreover, the image of this mapping is  $\{X \geq Y \geq Z \geq W\} \cap \{W = 1\} \subset \mathbb{R}_+^4$ , and can also be written  $\{(X, Y, Z, 1) \in \mathbb{R}^4 \mid X \geq Y \geq Z \geq 1\}$ .

Therefore each hyperplane that intersects the region  $\{X \leq Y \leq Z \leq W\}$  of the negative orthant can be represented uniquely by the intersection between a two-dimensional plane and the tetrahedron  $\{X \leq Y \leq Z \leq W\} \cap \{X+Y+Z+W = -1\} \cap \mathbb{R}_-^4$ , which in turn can be represented uniquely by the intersection between a two-dimensional plane and the “unbounded tetrahedron”  $\{(X, Y, Z, 1) \in \mathbb{R}^4 \mid X \geq Y \geq Z \geq 1\}$ . Moreover, we can map the set  $\{(X, Y, Z, 1) \in \mathbb{R}^4 \mid X \geq Y \geq Z \geq 1\}$  to  $\mathbb{R}^3$  by simply projecting on the  $XYZ$ -space. The result is shown in Fig. 8 and Fig. 9.

Then the toric differential inclusion  $\mathcal{T}_4$  can be represented by a such a set of planes in the region  $\{(X, Y, Z) \in \mathbb{R}^3 \mid X \geq Y \geq Z \geq 1\}$ . (We don't need to consider all 24 such regions since we have assumed that  $\mathcal{L}_4$  is symmetric with respect to linear transformations given by permutations of the coordinate axes.)

Note that, without loss of generality, we can assume that  $\mathcal{T}_4$  also contains additional horizontal “unbounded triangles”  $\{(X, Y, Z) \in \mathbb{R}^3 \mid X \geq Y \geq Z \geq 1, Z = \text{constant}\}$  through all the intersection points of planes in Fig. 8, and additional non-horizontal triangles connecting these intersection points, such that all the regions bounded by line segments are simplicial (i.e., tetrahedral), as illustrated in Fig. 10. (Like in the previous section, this means that  $\mathcal{T}_4$  is no longer a hyperplane-generated toric differential inclusion, but is now a general toric differential inclusion.)

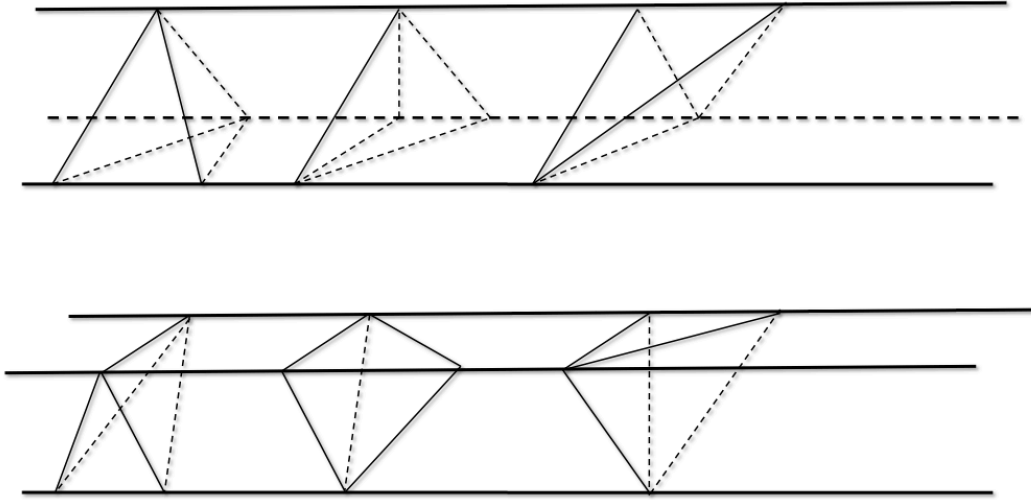


Figure 10: A partition of  $\mathcal{D}_3$ , analogous to the partition of  $\mathcal{D}_2$  from in the previous section, uses tetrahedra instead of triangles. Here we show only two representative “tunnels” in this partition, and the six different types of tetrahedra that may occur, depending on the positions of the vertices of the front face and the back face. Note that in Fig.4(c) we also had two types of triangles (with the horizontal edge on the bottom or on the top). This difference is reflected here in the difference between the top three and the bottom three tetrahedra.

In order to describe a method that allows us to construct a zero-separating surface for  $\mathcal{T}_4$ , let us revisit the construction of a zero-separating surface for  $\mathcal{T}_3$  in the previous section, to emphasize some key ideas.

If we look again at Fig. 5, we can interpret it as follows. On the left-side boundary of the domain  $\mathcal{D}_2$  we had two types of curve patches, i.e., the *1d-flat patches*<sup>34</sup>, and the *0d-flat patches*<sup>35</sup>.

Then, if the 1d-flat patches are short enough, and if the whole left-side

<sup>34</sup> By *1d-flat patches* we mean the parts of the left-side boundary curve near some vertices, which give rise to the shaded layers in the partition of  $\mathcal{D}_2$  shown in Fig. 5. The proximity of the vertices impose that these curve patches are straight line segments.

<sup>35</sup> By *0d-flat patches* we mean the parts of the left-side boundary curve that are not close to vertices, and give rise to the white layers in the partition of  $\mathcal{D}_2$  shown in Fig. 5. Some of these patches may actually be flat (i.e., straight line segments), but there is nothing in our construction that requires them to be flat.



boundary curve is faithful, then the construction described in the previous section is possible.

We can think of this construction systematically as follows. For each 1d-flat patch we have constructed a *polygonal line of 1d-flat patches*<sup>36</sup>, which is the image through the function  $\varphi$  of the corresponding shaded layer in the partition of  $\mathcal{D}_2$  shown in Fig. 5. Similarly, for each 0d-flat patch we have constructed a *polygonal line of 0d-flat patches*. For both types of polygonal lines of patches the construction is similar: the patches are continued from left to right in the attracting direction of a surface represented by a solid line segment, and they “turn” in a different direction along the surface represented by a dotted line segment.

A key property that makes this construction work is the fact that the two different types of polygonal lines of patches match perfectly along their common boundaries. On the other hand, we can see in Fig. 5 that the polygonal line of 0d-flat patches “turns” (i.e., encounters dotted lines) more times than the polygonal line of 1d-flat patches. The reason their boundaries still match is the following: even though the polygonal line of 1d-flat patches does not turn as many times (e.g., does not turn in the neighborhoods of points where solid lines intersect), its *boundary curves* do turn<sup>37</sup>.

Note that all we needed in the previous section in order to construct the polygonal lines of patches described above were the two different kinds of dotted lines. One way to think about our choice of a configuration of dotted lines as shown in Fig. 5 is the following. We can first choose “midpoints” for all the horizontal solid line segments, and decide that the thick dotted lines will pass through these midpoints. Once we have the thick dotted lines, we can also construct the intersections between them and the thin horizontal dotted lines. These intersection points are important, since the only other remaining dotted lines (the non-horizontal ones) pass through these points. We can construct these lines for example by connecting the intersection points with the triangle vertex that lies on the opposite side.

---

<sup>36</sup> We call it a *polygonal line of 1d-flat patches* because we construct it in a way that is similar to a polygonal line, except that a polygonal line starts with a point, and then advances along some straight lines, while a “polygonal line of 1d-flat patches” starts with a 1d-flat curve  $\mathcal{C}_1$ , then builds a surface patch by advancing along straight parallel lines until we reach another curve  $\mathcal{C}_2$  at the intersection with some surface, then builds another surface patch by advancing along another set of straight parallel lines, and so on.

<sup>37</sup> and even though the boundary curves turn, they still remain part of the same 1d-flat patch.

We now construct a zero-separating surface for  $\mathcal{T}_4$  based on the idea of polygonal lines of patches. We need to describe “dotted surfaces” (i.e., surfaces that sub-partition  $\mathcal{D}_3$ , and play the role that the dotted lines have played for sub-partitioning  $\mathcal{D}_2$  in Fig. 5) for the tetrahedral partition of the three-dimensional domain  $\mathcal{D}_3$  illustrated in Fig. 9 and Fig. 10.

We construct the dotted surfaces as follows. First, like in the 3d case, we choose *midpoints*<sup>38</sup> for all the horizontal line segments in the tetrahedral subdivision of  $\mathcal{D}_3$ . For example, in Fig. 10 (where we show just two representative tunnels within  $\mathcal{D}_3$ ) there will be one such midpoint on each line segment along the six horizontal half-lines shown there. Note that, in order to make this figure more clear, we have omitted many other tetrahedra that are also inside these same two tunnels (since, according to our construction,  $\mathcal{D}_3$  is partitioned by tunnels, and each tunnel is partitioned by tetrahedra).

Then, once we have the midpoints, we also construct *mid-curves*<sup>39</sup> along the  $X$ -direction tetrahedral faces<sup>40</sup>. Each mid-curve connects a point on the boundary of its adjacent *midpoint turning patch*<sup>41</sup> with the opposite vertex of the  $X$ -direction tetrahedral face that contains the mid-curve.

Once we have specified the midpoints and the mid-curves as described above, there is a unique way to build the polygonal lines of 2d-flat patches and the polygonal lines of 1d-flat patches.

Finally, we construct a *mid-surface*<sup>42</sup> within each tetrahedron, and it gives us a unique way to build the polygonal lines of 0d-flat patches, and therefore finish the construction of a zero-separating surface for the toric differential inclusion  $\mathcal{T}_4$ .

---

<sup>38</sup>we need these midpoints to be able to specify the turning points of the *polygonal lines of 2d-flat patches* that we will construct later.

<sup>39</sup> the mid-curves will specify the turning points of the *polygonal lines of 1d-flat patches*

<sup>40</sup> The  $X$ -direction tetrahedral faces are faces that contain the direction of the  $X$ -axis. Each tetrahedron contains exactly two such faces, and they are adjacent to a common horizontal edge, so they both have an adjacent midpoint that we constructed previously. The other two faces are called *back face* and *front face*, as seen in the direction of the construction, i.e, in the  $X$ -direction. The back face and the front face intersect in an edge which is called the *hinge edge* of the tetrahedron.

<sup>41</sup> a midpoint turning patch is the vertical patch that passes through a midpoint and along which the polygonal line of 2d-flat patches turns. Each  $X$ -direction tetrahedral face intersects exactly one midpoint turning patch.

<sup>42</sup>the mid-surface of a tetrahedron is a surface patch that lies approximately half-way between the back face and the front face of the tetrahedron, and it connects the hinge edge with the boundaries of the polygonal lines of 1d-flat patches and 2d-flat patches that intersect that tetrahedron.

As a final remark, let us also notice that there is another way to describe the above construction, as follows. For each tetrahedron in the subdivision of  $\mathcal{D}_3$ , we choose a midpoint of its *advance edge*<sup>43</sup> and then construct two “dotted lines” that start at this midpoint and go into the two faces of the tetrahedron that contain the advance edge<sup>44</sup>. Then the “dotted surface” of the tetrahedron is a triangular surface<sup>45</sup> that partitions the tetrahedron into two parts<sup>46</sup>. Two edges of the dotted surface are the dotted lines we mentioned above, and the third edge is the hinge edge of the tetrahedron. The dotted surface fills in the space in between its three edges according to the following rules: (i) the *midpoint* must be contained in the *midpoint turning patch* of the polygonal lines of 2d-flat patches, and the part of the midpoint turning patch that is contained in this tetrahedron must be contained in the dotted surface, (ii) the *mid-curve* must be contained in the *mid-curve turning patch* of the polygonal lines of 1d-flat patches, and the part of the mid-curve turning patch that is contained in this tetrahedron must be contained in the dotted surface, and (iii) the dotted surface is “vertical enough”, in the sense that approximately horizontal line segments intersect it in at most one point.

Condition (i) is trivial to enforce. To enforce condition (ii) we have to make sure that we do not allow the two mid-curve turning patches to intersect near the hinge edge. Finally, notice that (by moving the construction of the zero-separating surface close enough to the origin) we can assume that the turning patches are as thin as we wish, so the fitted surface is as close to the half-distance triangle between the back face and the front face. Therefore condition (iii) can also be satisfied.

Our next focus will be to construct a *faithful* zero-separating surface<sup>47</sup> for the 4d toric differential inclusion  $\mathcal{T}_4$ .

---

<sup>43</sup>the advance edge of a tetrahedron is its only edge in the horizontal direction (i.e., in the direction of the  $X$ -axis).

<sup>44</sup>these two faces are the horizontal faces of the tetrahedron.

<sup>45</sup>it is triangle-shaped, but it is not flat.

<sup>46</sup> Recall that the dotted surface has to serve as “turning surface” for the three kinds of polygonal lines of patches. The dotted surface has to partition the tetrahedron into two parts, one containing the back face, and one containing the front face. Then we have a “back half” and a “front half” of the tetrahedron, and in the back half the polygonal lines of patches advance in the attracting direction of the back face, and in the front half the polygonal lines of patches advance in the attracting direction of the front face.

<sup>47</sup> because it will be the starting point for a construction of zero-separating surface for a 5d toric differential inclusion  $\mathcal{T}_5$ , in the next section.

Recall that we have constructed a faithful zero-separating surface for the 3d toric differential inclusion  $\mathcal{T}_3$  in the previous section, essentially by building a slightly smaller triangle inside each triangle of the subdivision of  $\mathcal{D}_2$ , in a special way that makes all of the vertices of these smaller triangles align with each-other along turning patches and along some attracting directions (see Fig. 10).

Surprisingly, although this simple approach worked well in  $\mathbb{R}^3$ , *it fails to work*<sup>48</sup> in  $\mathbb{R}^4$ . Therefore, we need a new way of constructing a *faithful* zero-separating surface for  $\mathcal{T}_4$ , which will also generalize to higher dimensions.

A method that accomplishes this is the following. After we have subdivided the domain  $\mathcal{D}_3$  of  $\mathcal{T}_4$  into tetrahedra, we *further subdivide* each tetrahedron by choosing several points along its advance edge and connecting them with its hinge edge, and making sure that the first such point is very close to the back face, the last such point is very close to the front face, and there is at least one more point between them.

Denote this new polygonal fan by  $\mathcal{F}'_4$ , and its associated toric differential inclusion by  $\mathcal{T}'_4$ , and consider a zero-separating surface for  $\mathcal{T}'_4$  constructed close enough to the origin. Then, for each tetrahedron of  $\mathcal{T}_4$ , the normals to this zero-separating surface for  $\mathcal{T}'_4$  at points that are not in any uncertainty region of  $\mathcal{T}_4$  belongs to the *interior* of the attracting cone of that tetrahedron of  $\mathcal{T}_4$ . Therefore, this zero-separating surface for  $\mathcal{T}'_4$  is a *faithful* zero-separating surface for  $\mathcal{T}_4$ .

## 4.5 General ( $n$ -dimensional) toric differential inclusions

The constructions we have described in the previous sections can be carried on analogously in higher dimensions. To build a zero-separating surface for an  $n$ -dimensional toric differential inclusion  $\mathcal{T}_n$ , we first subdivide the simplicial domain

$$\{X_1 + X_2 + \dots + X_n = -1\} \cap \mathbb{R}_-^n$$

into  $n!$  subdomains given by specific orderings of the logarithmic coordinates  $X_1, \dots, X_n$ . Then we take the representative subdomain

$$\{X_1 \leq X_2 \leq \dots \leq X_n\} \cap \{X_1 + X_2 + \dots + X_n = -1\} \cap \mathbb{R}_-^n$$

and map it to the unbounded simplicial domain  $\mathcal{D}_{n-1} \subset \mathbb{R}_+^{n-1}$ .

---

<sup>48</sup> It fails because the system of restrictions given by these alignments is overdetermined in  $\mathbb{R}^4$ .

Then we subdivide  $\mathcal{D}_{n-1}$  into  $(n-1)$ -dimensional simplices (similar to our decomposition of  $\mathcal{D}_2$  into triangles and of  $\mathcal{D}_3$  into tetrahedra) and assume that we have already constructed a “left-side boundary condition” for a zero separating surface on  $\mathcal{D}_{n-1}$ <sup>49</sup>.

The simplices of  $\mathcal{D}_{n-1}$  can be organized along “tunnels” that start at simplices on the left-side boundary of  $\mathcal{D}_{n-1}$  and go in the  $X_1$ -direction. This provides a lexicographic-type *ordering* of all the simplices of  $\mathcal{D}_{n-1}$ , based on the ordering of simplices of  $\mathcal{D}_{n-2}$  and the order of increasing  $X_1$  values in simplices within the same tunnel in  $\mathcal{D}_{n-1}$ .

Then, we build a zero-separating surface for  $\mathcal{T}_n$  by constructing one piece of the surface for each simplex of  $\mathcal{D}_{n-1}$ , in the order described above. The construction is based on *polygonal lines of patches*, like in the previous section. The turning sets for the polygonal lines of patches are given by a “dotted surface” constructed like in the previous section: for each simplex of  $\mathcal{D}_{n-1}$ , we first choose a midpoint of its advance edge, then we construct boundary patches of the dotted surface on all the facets<sup>50</sup> of the simplex that contain the advance edge, and then connect these boundary patches with the codimension-two face that is opposite the advance edge.

Finally, we can also obtain *faithful* zero-separating surfaces for  $\mathcal{T}_n$ , by subdividing each simplex of  $\mathcal{D}_{n-1}$  into several simplices, given by a choice of at least three points along the advance edge of the simplex, as explained in the previous section. Faithful zero-separating surfaces for  $n$ -dimensional toric differential inclusions serve as left-side boundary conditions for zero-separating surfaces for  $(n+1)$ -dimensional toric differential inclusions, and so on.

## 5 Proof of the global attractor conjecture

Consider a toric dynamical system<sup>51</sup>  $\mathbf{T}_n$  in  $\mathbb{R}_+^n$ , and fix some  $0 < \varepsilon \ll 1$ . From the work of Horn and Jackson [14] we know that  $\mathbf{T}_n$  has a globally

---

<sup>49</sup> If we partition  $\mathcal{D}_{n-1}$  into half-lines in the direction of the  $X_1$ -axis, then the “left-side boundary” of  $\mathcal{D}_{n-1}$  is the set of boundary points of these half-lines. The left-side boundary of  $\mathcal{D}_{n-1}$  is essentially a copy of  $\mathcal{D}_{n-2}$ , and the zero-separating surface constructed along it is based on previously constructed *faithful* zero-separating surface for a  $(n-1)$ -dimensional toric differential inclusion.

<sup>50</sup> this relies on the construction of the dotted surface in the  $(n-1)$ -dimensional case

<sup>51</sup>i.e., a dynamical system of the form (1) that has a positive equilibrium that satisfies the vertex-balance identity (3).

defined strict Lyapunov function within any linear invariant subspace. Also, we know [8] that there exist level sets of this Lyapunov function that allow us to build an invariant region  $\mathcal{R}_n^0$  for  $\mathbf{T}_n$  in  $\mathbb{R}_+^n$  such that

$$\{x \in \mathcal{R}_n^0 | \text{dist}(x, 0) < \varepsilon_0\} = \emptyset \text{ and } \{x \in \mathcal{R}_n^0 | \text{dist}(x, 0) > 1/\varepsilon_0\} = \emptyset,$$

for some  $\varepsilon_0 > 0$ , and such that the hypercube  $\mathcal{H}_\varepsilon = [\varepsilon, \frac{1}{\varepsilon}]^n$  is contained inside  $\mathcal{R}_n^0$ .

Then we proceed as in the Section 7 of [1], and build an invariant region  $\mathcal{R}_n^1 \subset \mathcal{R}_n^0$  that also contains  $\mathcal{H}_\varepsilon$  and does not have any points at distance less than  $\varepsilon_1 > 0$  from the *coordinate axes* of  $\mathbb{R}_+^n$ , by using the fact that, in a neighborhood of each coordinate axis of  $\mathbb{R}_+^n$ , the  $n$ -dimensional toric dynamical system  $\mathbf{T}_n$  restricted to  $\mathcal{R}_n^0$  can be regarded as an  $(n - 1)$ -dimensional  $k$ -variable toric dynamical system. This allows us construct  $\mathcal{R}_n^1$  by excluding  $n$  cylindrical neighborhoods of the coordinate axes from  $\mathcal{R}_n^0$ . See also Fig.7.1 in [1].

In the next step we build an invariant region  $\mathcal{R}_n^2 \subset \mathcal{R}_n^1$  that contains  $\mathcal{H}_\varepsilon$  and does not have any points at distance less than  $\varepsilon_2 > 0$  from the *coordinate planes* of  $\mathbb{R}_+^n$ , and then we build an invariant region  $\mathcal{R}_n^3 \subset \mathcal{R}_n^2$  that contains  $\mathcal{H}_\varepsilon$  and does not have any points at distance less than  $\varepsilon_3 > 0$  from the *coordinate 3-spaces* of  $\mathbb{R}_+^n$ , and so on.

In the end<sup>52</sup> we obtain a bounded invariant region  $\mathcal{R}_n^{n-1}$  for  $\mathbf{T}_n$  that contains  $\mathcal{H}_\varepsilon$  and does not contain any points at distance less than  $\varepsilon_{n-1} > 0$  from the boundary of  $\mathbb{R}_+^n$ . Therefore, for each initial condition  $x_0 \in \mathbb{R}_+^n$  we can construct an invariant region  $\mathcal{R}_n^{n-1}$  above such that  $x_0 \in \mathcal{R}_n^{n-1}$ . Then we can use LaSalle invariance [19, 20] for the global strict Lyapunov function mentioned above to conclude that, within any linear invariant subspace, any trajectory of  $\mathbf{T}_n$  converges to its vertex-balanced positive equilibrium point.

## Acknowledgements

We thank Uri Alon, David Anderson, Murad Banaji, Lev Borisov, Andrei Caldararu, Martin Feinberg, Manoj Gopalkrishnan, Jeremy Gunawardena,

---

<sup>52</sup> Note that we can use the same construction as above to show that any bounded trajectory of a  $k$ -variable toric dynamical system is persistent (and, in particular, any bounded trajectory of a  $k$ -variable weakly reversible mass-action dynamical system is persistent), except that we also have to construct  $\mathcal{R}_n^0$  using toric differential inclusions, instead of using the Lyapunov function. We will discuss this and more general results about persistence and permanence of  $k$ -variable toric dynamical systems in future work [30, 31].

Morris Hirsch, Heinz Koeppl, Ezra Miller, Fedor Nazarov, Casian Pantea, Joel Robbin, Anne Shiu, Eduardo Sontag, Frank Sottile, and Bernd Sturmfels for very useful comments and discussions.

## References

- [1] G. Craciun, F. Nazarov, C. Pantea, *Persistence and permanence of mass-action and power-law dynamical systems*, SIAM J. Appl. Math. 73:1, 305-329, 2013.
- [2] D.F. Anderson, A. Shiu, *The dynamics of weakly reversible population processes near facets*, SIAM J. Appl. Math. 70, 1840-1858, 2010.
- [3] D.F. Anderson, *A proof of the Global Attractor Conjecture in the single linkage class case*, SIAM J. Appl. Math. 71:4, 2011.
- [4] David F. Anderson, Gheorghe Craciun, and Thomas G. Kurtz, *Product-form stationary distributions for deficiency zero chemical reaction networks*, Bull. Math. Biol. 72:8, 1947-1970, 2010.
- [5] D. Angeli, P. de Leenheer, and E.D. Sontag, *Persistence results for chemical reaction networks with time-dependent kinetics and no global conservation laws* SIAM J. Appl. Math. 71, 128-146, 2011.
- [6] M. Banaji, G. Craciun, *Graph-theoretic approaches to injectivity and multiple equilibria in systems of interacting elements*, Communications in Mathematical Sciences 7:4, 867-900, 2009.
- [7] P. Donnell and M. Banaji, *Local and global stability of equilibria for a class of chemical reaction networks*, SIAM J. Appl. Dyn. Syst. 12:2, 2013.
- [8] G. Craciun, A. Dickenstein, A. Shiu, B. Sturmfels, *Toric Dynamical Systems*, J. Symb. Comp., 44:11, 1551–1565, 2009.
- [9] M. Feinberg, *Complex balancing in general kinetic systems*, Arch. Rational Mech. Anal. 49, 187-194, 1972.

- [10] M. Feinberg, *Lectures on Chemical Reaction Networks*, written version of lectures given at the Mathematical Research Center, University of Wisconsin, Madison WI, 1979. Available at <http://www.crnt.osu.edu/LecturesOnReactionNetworks>
- [11] M. Feinberg, *Existence and uniqueness of steady states for a class of chemical reaction networks*, Arch. Rational Mech. Anal., 132, 311-370, 1995.
- [12] M. Feinberg, *Chemical Reaction Networks structure and the stability of complex isothermal reactors – I. The deficiency zero and deficiency one theorems*. Chem. Eng. Sci. 42:10, 2229-2268, 1987.
- [13] M. Gopalkrishnan, E. Miller, and A. Shiu, *A geometric approach to the global attractor conjecture*, SIAM Journal on Applied Dynamical Systems 13:2, 758-797, 2014.
- [14] F. Horn and R. Jackson, *General mass action kinetics*, Arch. Rational Mech. Anal. 47, 81-116, 1972.
- [15] F. Horn, *The dynamics of open reaction systems*, in Mathematical Aspects of Chemical and Biochemical Problems and Quantum Chemistry (Proc. SIAM-AMS Sympos. Appl. Math., New York), SIAM-AMS Proceedings, Vol. 8, Amer. Math. Soc., Providence, R.I., 125-137, 1974.
- [16] C. Pantea, *On the persistence and global stability of mass-action systems*, SIAM J. Math. Anal. Vol. 44, No. 3, 1636–1673.
- [17] G. Shinar and M. Feinberg, *Concordant chemical reaction networks*, Mathematical Biosciences 240, 92-113, 2012.
- [18] A. Shiu, B. Sturmfels, *Siphons in chemical reaction networks*, Bulletin of Mathematical Biology, 72:6, 1448-1463, 2010.
- [19] D. Siegel and D. MacLean, *Global stability of complex balanced mechanisms*, J. Math. Chem. 27:1-2, 89-110, 2004.
- [20] E.D. Sontag, *Structure and stability of certain chemical networks and applications to the kinetic proofreading model of T-cell receptor signal transduction*, IEEE Trans. Automat. Control, 46, 1028-1047, 2001.



- [21] G. Craciun and M. Feinberg, *Multiple equilibria in complex chemical reaction networks: I. The injectivity property*, SIAM J. Appl. Math. **65** 1526-1546, 2005.
- [22] G. Craciun and M. Feinberg, *Multiple equilibria in complex chemical reaction networks: II. The Species-Reaction graph*, SIAM J. Appl. Math. **66**, 1321-1338, 2006.
- [23] G. Craciun, Y. Tang and M. Feinberg, *Understanding bistability in complex enzyme-driven reaction networks*, PNAS **103**, 8697-8702, 2006.
- [24] H. L. Smith and P. Waltman, *Perturbation of a globally stable steady state*, Proc. Amer. Math. Soc. **127**, 447-453, 1999.
- [25] M. A. Savageau, E. O. Voit, *Recasting nonlinear differential equations as S-systems: a canonical nonlinear form*, Mathematical Biosciences **87**:1, 83-115, 1987.
- [26] J. Gunawardena, *Chemical Reaction Network Theory for in-silico biologists*, Lecture notes available online at <http://vcp.med.harvard.edu/papers.html>, 2003.
- [27] D. Cox, J. Little, H. Schenck, *Toric Varieties*, Graduate Studies in Mathematics **124**, American Mathematical Society, 2011.
- [28] W. Fulton, *Introduction to Toric Varieties*, Princeton University Press, Princeton, New Jersey, 1993.
- [29] R. T. Rockafellar, *Convex Analysis*, Princeton University Press, Princeton, New Jersey, 1970.
- [30] G. Craciun, *Toric Differential Inclusions and a Proof of the Persistence Conjecture*, in preparation.
- [31] G. Craciun, *Mass-action dynamical systems, polynomial systems, and power-law systems*, in preparation.